Densification mechanisms of haplogranite glasses as a function of water content and pressure based on density and Raman data

Elsevier Editorial System(tm) for Geochimica et Cosmochimica Acta

Manuscript Draft

Manuscript Number: W8995R3

Title: (W8995)Densification mechanisms of haplogranite glasses as a function of water content and pressure based on density and Raman data

Article Type: Article

Corresponding Author: Dr. Paola Ardia, Ph.D.

Corresponding Author's Institution:

First Author: Paola Ardia, Ph.D.

Order of Authors: Paola Ardia, Ph.D.; A Di Muro; D Giordano; D Massare; C Sanchez-Valle; M W Schmidt

Abstract: This study investigates the effect of pressure (1 atm - 2.5 GPa) and water (0.15, 2.7, 3.6 and 5.2 wt% H2O) on the network structure of alkali-rich alumino-silicate glasses synthesized at 1000 °C. Density increases linearly with pressure in the water-poor composition, while in the water-rich glasses and above 1.5 GPa densification decreases with pressure. Raman data suggest that several structural changes follow one upon another with increasing pressure and water content. The almost dry glasses undergo large modifications of the network ring structure with pressure, namely a decrease in average T-O-T angle, change in ring size statistics and possibly an increasingly homogeneous distribution of Al- and Si-rich domains at high pressure. Water dissolution favors a homogenization of ring sizes at low pressures. Pressure essentially induces a decrease in the average intertetrahedral angle and, above 1.5 GPa, a possible redistribution of Al/Si-rich regions. Pressure induces an increase in O-H bonding but decreases the O-H bond strength. The observed structural modifications are consistent with the decreasing net effect of pressure on viscosity as temperature and water increase through variation of the activation volume of viscosity.

Densification mechanisms of haplogranite glasses as a function of water content and pressure based on density and Raman data

P. Ardia[1*], A. Di Muro[2], D. Giordano[3], D. Massare[2], C. Sanchez-Valle[1], M.W. Schmidt[1]

1) Department of Earth Sciences, ETH, Sonneggstrasse 5, 8092 Zurich, Switzerland
2) Laboratoire de Géologie des Systèmes Volcaniques, IPGP UMR 7154, 4 Place Jussieu, 75005 Paris, France
3) Dipartimento di Scienze della Terra, Universita' degli Studi di Torino, Via Valperga Caluso 35, 10125 Torino, Italia

*) Corresponding author, paola.ardia@gmail.com

ABSTRACT

This study investigates the effect of pressure (1 atm – 2.5 GPa) and water (0.15, 2.7, 3.6 and 5.2 wt% H_2O) on the network structure of alkali-rich alumino-silicate glasses synthesized at 1000 °C. Density increases linearly with pressure in the water-poor composition, while in the water-rich glasses and above 1.5 GPa densification decreases with pressure. Raman data suggest that several structural changes follow one upon another with increasing pressure and water content. The almost dry glasses undergo large modifications of the network ring structure with pressure, namely a decrease in average T-O-T angle, change in ring size statistics and possibly an increasingly homogeneous distribution of Al- and Si-rich domains at high pressure. Water dissolution favors a homogenization of ring sizes at low pressures. Pressure essentially induces a decrease in the average intertetrahedral angle and, above 1.5 GPa, a possible redistribution of Al/Si-rich regions. Pressure induces an increase in O-H bonding but decreases the O-H bond strength. The observed structural modifications are consistent with the decreasing net effect of pressure on viscosity as temperature and water increase through variation of the activation volume of viscosity.

1. INTRODUCTION

The structural evolution of alkali and silica rich melts and glasses with pressure and dissolved total water contents (H_2O_T) is crucial for understanding the physical-chemical properties of silicic (rhyolitic, phonolitic or trachytic) magmas at crustal depths and, eventually, for modelling intrusive and eruptive processes. Considerable effort has been devoted to interpreting changes of bulk properties such as density and viscosity in Si-rich alumino-silicate melts in terms of short- and medium-range structural variations (Mysen et al., 1980a; Mysen and Virgo 1986; Matson et al:,

1986; Lange and Carmichael, 1987, 1989; Okuno et al, 1996; Zotov and Keppler, 1998; Zotov, 2003; Allwardt et al., 2007). Pressure, temperature and dissolved water content play contrasting roles on liquid structural rearrangement and physico-chemical properties. Density decreases with increasing temperature and bulk water content due to thermal expansivity and to the large molar volume of "water" (sum of hydroxyl OH and molecular water H_2O; Ochs and Lange, 1999; Richet et al., 2000). In haplogranite melts, water has a major effect on melt and glass properties and its solubility is a positive function of pressure, alkali ratio (Na/K) and, subordinately, of temperature (Holtz et al., 1992; Acosta-Virgil et al., 2005; Ardia et al., 2008). Conversely, compression results in network densification and a linear increase in bulk density (1 atm to 2 GPa, Kushiro, 1978; 2.6 to 5.3 GPa, Suzuki et al., 2002). Similarly, the viscosity of silicic melts is drastically affected by temperature, water-content and pressure (Shaw, 1963; Hess and Dingwell, 1996; Dingwell et al., 1996, Ardia et al., 2008; Giordano et al., 2008a, del Gaudio and Behrens, 2009; Hui et al., 2009). At high temperature, both the first compression applied to haplogranite melts and the first dissolution of H_2O induces a stronger decrease in viscosity than subsequent increments (Kushiro, 1978; Behrens and Schulze, 2003; Ardia et al., 2008). On the other hand, pressure increases the viscosity of hydrous rhyolites at low temperatures (Hui et al., 2009). Structural models designed to interpret the effect of pressure on the properties of alkali-bearing alumino-silicate melts must therefore explain the simultaneous linear density increase and the non-linear evolution of viscosity with increasing pressure at varying water content.

Kushiro (1978) interpreted the structural evolution of albitic and silica-rich melts with increasing pressure by analogy to the structural changes observed in crystals. In this model, a gradual change of Al-coordination from IV to VI is proposed at pressures below 1.0 GPa. Alternatively, Sharma et al. (1979) suggested that the observed decrease in melt viscosity with pressure relates to ordering or reorganization of the three-dimensional network. More specifically, Seifert et al. (1982) and Mysen et al. (1983) proposed that the decrease in average T-O-T angles with pressure determines the counterintuitive decrease in viscosity with increasing density. Hochella and Brown (1985) summarized the investigations on albitic to jadeitic compositions and only report minor changes in Raman spectra up to 4.0 GPa thus discarding the possibility that Al-coordination changes would be responsible for the observed melt densification and viscosity changes. This has been further confirmed by more recent Raman spectroscopy studies (Okuno et al., 1999; Reynard et al., 1999; Shimoda et al., 2004; Champagnon et al., 2008), which investigate the effect of pressure on water-poor natural obsidians and dry synthetic glass analogues (silica, anorthite and albite glass compositions) between 1 atm and 25 GPa. Spectral analysis suggests that the densification process operates through two main mechanisms, a decrease in the intertetrahedral angles (T-O-T), and a re-organization of the connected rings forming the alumino-silicate network.

In this study, we investigate the effect of pressure on the structure of water-poor (H_2O_T: 0.15 wt%) and water-rich (H_2O_T: 2.7-5.2 wt%) haplogranite glasses ($Qz_{36}Ab_{37}Or_{27}$) combining density measurements and Raman spectroscopy on isobarically quenched glasses from 1000 °C at five different pressures (0.5, 1.0, 1.5, 2.0 and 2.5 GPa). High pressure glasses are compared to a reference water-poor glass relaxed at 1 atm. Because of similarities in composition, our vibrational data are interpreted by comparison with the extensively investigated (Na,K)AlO_2-SiO_2 system (Mysen et al., 1980a; Seifert et al., 1983) with special reference to silica (Champagnon et al., 1996; Okuno et al., 1999; Champagnon et al., 2008) and albite composition glasses (Kushiro, 1978; Romano et al., 2001; Suzuki et al., 2002; Behrens and Schulze, 2003; Poe et al., 2006) whose structure and physical properties are known over a broad range of pressures and temperatures.

Quenching is presumed to freeze the densest configuration attained at high pressure and the water-speciation (OH/H_2O_m ratio) (Hui et al., 2008) at the glass transition (T_g), while the purely elastic part of the deformation is eventually released during decompression. In glasses, it has been proposed that water speciation does not depend on pressure (Richet et al., 2000). This conclusion has been recently questioned for rhyolites by Hui et al. (2008), who observed a variation of water speciation with quench pressure and employed the speciation to calculate viscosities at various pressures (Hui et al., 2009). As we will show, our data suggest that densification involves a set of mechanisms, which change with increasing pressure and water content and affect the molar volume of H_2O, at least at pressures above 1.5 GPa.

2. GLASS SYNTHESIS AND QUENCH CONDITIONS

2.1. Synthesis

HGG haplogranite glasses ($Na_{0.56}K_{0.38}Al_{0.95}Si_{5.19}O_{12.2}$) are silica-rich (Si/(Si+Al) = 0.85) and slightly peralkaline ((Na+K)/Al = 1.04; Na/K = 1.5). The starting glasses with different water contents were synthesized in a hot isostatic press (HIP) and one of those was dehydrated using a concentric cylinder technique (Ardia et al., 2008). The resulting four compositions are from the same batches used for viscosity measurements at high pressure and temperature (Ardia et al., 2008), for elasticity measurements using Brillouin spectroscopy and for ^{27}Al NMR studies (Malfait et el., 2011, 2012). Samples HGG0, HGG3, HGG4 and HGG5 correspond to haplogranite glasses with total dissolved water contents of 0.15, 2.7, 3.6 and 5.2 wt%, respectively. Water contents of the bulk glasses were determined by Karl-Fischer titration at ETH Zurich (KFT, Behrens and Stuke, 2003). Glass homogeneity was confirmed by micro-FTIR and micro-Raman analyses in Paris (Di Muro et al., 2006a) for water content, and with electron microprobe (JEOL JXA 8200) analyses of bulk

compositions at ETH Zurich (Ardia et al., 2008). The glass samples for spectroscopic investigation were prepared in an end-loaded piston cylinder by melting the starting glasses from a previous synthesis (Ardia et al., 2008) in Pt capsules at various pressures (0.5-2.5 GPa) and a constant temperature of 1000 °C. Complete homogenization and relaxation were assured by keeping the melts at run condition for 12 h for water-rich samples (HGG 3, 4, 5) and for 2 h for the nearly anhydrous synthesis HGG0, because the synthesis using concentric cylinder already ensures homogenization (Ardia et al., 2008). Samples were isobarically quenched by manually maintaining pressure. Although small pressure drops cannot be excluded, they cannot be precisely evaluated and are assumed to be similar for each run. The cooling rate of the end-loaded piston cylinder is 150-200 °C/s and is assumed to be constant for each experiment. Recovered glasses were optically examined and minor quench crystallization was identified at the rims of some water-rich glasses close to the glass-capsule interface. Thin glass chips were double side polished with parallel faces for micro-Raman studies. Only crystal-free glassy areas not affected by cracks or bubbles were analyzed.

2.2. Influence of pressure on glass transition temperature

The glass transition (T_g) is a kinetic boundary between the mechanical response to an applied stress of a liquid-like viscous and solid-like elastic material, and corresponds to the temperature of quenching of the liquid structure upon cooling (Dingwell and Webb, 1990; Gottsmann et al., 2002). The glass transition temperature is associated to specific viscosity values at fixed cooling rate, but is compositional dependent (Morizet et al., 2007; Giordano et al., 2008b). The temperature interval across the glass transition depends on composition, thermal history (cooling rate) and experimentally, upon the timescale of the investigation method (Moynihan et al., 1976; Dingwell and Webb, 1990; Moynihan, 1995; Giordano et al., 2005, 2008b). The structural relaxation depends on processes affecting both the viscous and elastic components (Maxwell, 1867) and, as a consequence, its mechanical and thermodynamic properties.

The glass transition depends on the cooling rate (q) applied to a system, and can be inferred from the apparent equilibrium temperature (T_{ae}) for hydrous rhyolite melts using the relationship (Scherer, 1984; Stevenson et al., 1995; Toplis et al., 2001; Gottsmann et al., 2002; Sipp and Richet, 2002; Zhang et al., 2003):

$$\log \eta_{T_g} \approx \log \eta_{T_{ae}} = 11.45 - \log q \qquad (1)$$

where η is the viscosity in Pa·s (Hui et al., 2009). Using a quench rate of q= 150 °/s we obtain a viscosity of $10^{9.3}$ Pa·s. This viscosity is then used to recalculate T_{ae} applying available models for the effect of pressure on the viscosity of rhyolitic liquids (Ardia et al., 2008 and Hui et al., 2009). The model of Ardia et al. (2008) is derived from measured viscosities of < 10^7 Pa·s for hydrous and of <

10^8 Pa·s for low water content rhyolitic liquids. The model of Hui et al. (2009) applies to high viscosities (10^{10}-10^{12} Pa·s) but is not accurate at low water contents (< 0.80 wt% H_2O). The viscosity corresponding to the glass transition of the HGG glasses ($10^{9.3}$ Pa·s) is intermediate between the calibration ranges of both Ardia's (2008) and Hui's (2009) models. The temperature of freezing upon constant cooling (quench temperature) (Table 1) calculated with the two models differ significantly for high water contents. This discrepancy occurs because the Ardia et al. (2008) model predicts a decrease in quenching temperature with pressure, following the trend derived from low water content glasses, whereas the Hui et al. (2009) model suggests a modest increase in quench temperature with pressure (Table 1). In this study, we retain the quench temperatures for the low water content glass as predicted by Ardia et al. (2009) and for the high water content glasses as calculated from Hui et al. (2009). For comparison, we have evaluated T_{ae} for a viscosity of $\eta=10^{12}$ Pa·s conventionally assumed as the viscosity of the glass transition for dry glasses at 1 atm (Dingwell and Webb, 1990) (Table 1). In summary, T_{ae} decreases with increasing pressure for nearly anhydrous compositions (Ardia's model), whereas at increasing water contents T_{ae} increases with pressure (Hui's model). In both models, T_{ae} decreases with water addition at a given pressure (Table 1).

3. METHODS

3.1 Density measurements

Density measurements were performed in a pyrex pycnometer by immersion of small glass chips of cylindrical shape and ca. 1 mm diameter in a heavy liquid (Na-polytungstate solution). This method requires a dilution of the solution with distilled water until neutral buoyancy of the immersed glass chip is attained at room temperature. Care was taken to verify that no bubbles adhere to floating glasses that could produce erroneous density measurements. The duration of the measurements (minutes to tens of minutes) was optimized to prevent the evaporation of distilled water and to attain neutral buoyancy. Density is then determined by calculating that of the diluted heavy liquid. The accuracy of this method is estimated to ± 0.001-0.002 g/cm^3 for 0.5 mg of sample (Popel et al., 2011). Table 2 reports average errors (1σ standard deviation) of all measurements.

3.2 Raman spectroscopy

Raman spectra of HGG glasses (average of 3 full spectra for each glass) were obtained at room conditions in confocal configuration using two micro-Raman apparatus: a LabRam HR 800 dispersive spectrometer (Jobin-Yvon®) at LADIR laboratory (UPMC Paris VI, France) and an inVia

Reflex dispersive spectrometer (Renishaw®) at Pierre-Süe laboratory (CEA, France). Non-polarized spectra of all glass samples were acquired with the Renishaw system using a diode laser (λ = 488.0 nm) as excitation source. A sub-set of non-polarized and polarized spectra was collected with the LabRam HR800 system using the 488.0 nm line of an argon ion laser. Both systems are equipped with a Peltier-cooled multichannel CCD detector and a microscope that allows observation of the sample, focusing of the laser beam at the surface of the sample, and collection of the Raman signal in backscattering geometry. All spectra were collected using 1800 grooves/mm grating and edge filters were used to suppress the dominant Rayleigh scattering. These conditions permitted to optimize the intensity yield and provide the spatial resolution (ca. 1 μm) necessary to minimize the influence of physical heterogeneities such as crystals, cracks, and bubbles. The LabRam setup provides a spectral resolution of 0.6 cm^{-1}/pixel in the 150-1400 cm^{-1} range due to the long focal length (800 mm) whereas a resolution of 1.5 cm^{-1}/pixel is achieved with the Renishaw spectrometer (250 mm focal). The spectral resolution slightly decreases at higher frequencies (3000 - 3800 cm^{-1}) to 1.0 and 2.0 cm^{-1}/pixel for the LabRam and Renishaw systems, respectively. With the LabRam system, acquisition times per spectrum at a power of 7.5 mW were 1000 s for the nearly anhydrous glasses and 250 s for the water-rich glasses to avoid damage and instability of the sample. Measurements with the Renishaw system were conducted using about 3 mW power at the sample surface and reduced exposure times to 30 s for the high frequency domain (2800-4100 cm^{-1}) and to 40 s for the low frequency domain (150-1400 cm^{-1}).

3.2.1. Data treatment

High resolution polarized spectra were collected to identify the main Raman features and to accurately determine band positions and widths, and the depolarization ratios ($\rho_{dr}=I_{VH}/I_{VV}$). A polarized band is associated with a totally symmetric vibration ($\rho_{dr}=0$), while a slightly asymmetric vibration results in depolarized bands. Conversely, the analysis of non-polarized data allows assessing and correlating the general evolution of spectra with the synthesis conditions of the samples. Raw scattered intensities I(ν)(I_{obs}^{Stokes}in equation 2) in Raman spectra (Fig. 1a) are frequency- and temperature-dependent, with the intensities of low-frequency bands being enhanced relative to those at high-frequencies. Therefore the raw Raman intensities I_{obs}^{Stokes} were corrected to obtain the reduced spectra I_{corr}^{Stokes} (Long, 1977; Brooker et al., 1988; McMillan and Wolf, 1995; Long, 2002) that provide representative intensities for all vibrational modes (Fig1b). A linear baseline (Fig. 1a) was first fitted to the high-frequency domain (>1200 cm^{-1}) and subtracted from all spectra before correcting them according to the relation:

$$I_{coor}^{Stokes} = I_{obs}^{Stokes} \cdot \nu^{*3} \cdot (1 - e^{-\frac{hc\nu}{kT}}) \cdot \frac{\nu}{(\nu^* - \nu)^4} \qquad (2)$$

where I_{obs}^{Stokes} is the measured intensity, ν* the wavenumber of the incident laser light, ν the measured wavenumber, both in cm^{-1}, *T* temperature in K, *c* the speed of light (ms^{-1}) and *k* ($1.38\ 10^{-23}\ JK^{-1}$) and *h* ($6.63\ 10^{-34}$ Js) the Boltzmann and Planck constants, respectively (Fig. 1b). In the analysis of the OH-stretching domain (2900-4000 cm^{-1}), a cubic baseline was subtracted (Fig. 2) (Zajacz et al., 2005; Behrens et al., 2006; Di Muro et al., 2006a). All spectra were normalized to the intensity of the most intense observed band at ca. 490 cm^{-1} and smoothed using the Loess algorithm (3%) (Figs. 1c, 2) before performing spectral deconvolution using the software PeakFit(R). All intensities and intensity changes reported in the following are normalized intensities (N.I.).

4. RESULTS

4.1. Density

Figure 3a reports the measured densities of HGG glasses (Table 2), compared with that of dry albitic glasses (Kushiro, 1978), and calculated densities of rhyolitic glasses following Withers and Behrens (1999). Densities increase linearly with quench pressure for the dry albitic and almost dry haplogranitic (HGG0) compositions, following parallel trends. The density of HGG0 is 1.4-2.5 % lower than that of dry albitic glass in the investigated pressure range. The densities of hydrous haplogranitic glasses also increase linearly with pressure up to 1.5 GPa for HGG3 and HGG4, and to 1.0 GPa for HGG5, respectively. Above these pressures, density increase levels off.

Figure 3b shows the evolution of glass densities as a function of water content. Density decreases linearly with increasing dissolved H_2O at a given pressure, and with a rate that is similar over the whole explored pressure range. Withers and Behrens (1999) suggested that quench rate, together with water content, influence glass densities. In fact, lower densities in rhyolites are found for high quench rates (>100 °/s; at 0.3 GPa), while slower cooling (ca. 100-150 °/min; at 0.5 GPa) results in slightly higher glass densities. Our density data on HGG glasses from 0.5 GPa are very close to those of Withers and Behrens (1999) for fast quenched rhyolites from 0.3 GPa, in agreement with the finding that fast quench glasses have lower densities. The almost constant difference between our glasses quenched at various pressures and the rhyolitic glasses obtained by slow cooling (Withers and Behrens, 1999) indicates that our glasses retained the effect at high pressure upon cooling.

Pressure increases the density of glasses with the exception of one hydrous glass of the HGG4 set, where the glass synthesized at 2.5 GPa has a lower density than that at 1.5 GPa (Fig. 3a). This

behavior may be related to partial crystallization and cracking upon quench and therefore the spectroscopic properties of the HGG4/2.5 GPa sample will not be discussed further.

4.2. Partial molar volumes of water

Figure 4 and Table 3 show the calculated ambient molar volumes for HGG glasses synthesized at various pressures, together with data for a set of albitic and rhyolitic compositions (Richet et al., 2000). Molar volumes derived from high-pressure synthesis are up to 6.5 % lower than those derived from low-pressure runs and are very similar for the albitic, most of the rhyolitic and HGG glasses (Table 3). Only the rhyolitic glasses of Withers and Behrens (1999) have an opposite trend that would result from the inverse relation of density as a function of synthesis pressure caused by different quench rates. The linear variation of molar volume as a function of the molar fraction of dissolved water (Fig. 4) indicates an almost constant partial molar volume of water (V^*_{H2O}), within experimental uncertainty (Table 3). This is in agreement with Richet et al. (2000) who reported a constant V^*_{H2O} of 12.0 ± 0.5 cm^3/mol for albitic and rhyolitic compositions. In this study, a V^*_{H2O} of 12.1 ± 1.0 cm^3/mol is obtained for pressures to 1.5 GPa, in agreement with Richet et al. (2000) (Fig. 4; Table 3). However, the V^*_{H2O} increases to 13.7 ± 1.0 cm^3/mol at 2.5 GPa and is associated with a smoother increase in density at high pressure.

4.3. Spectra analysis

4.3.1. Raman spectra general features and deconvolution strategy

The unpolarized Raman raw spectra of HGG glasses display broad bands typical of amorphous materials (Fig. 5). Three main envelopes can be identified in the low- (150-650 cm^{-1}; LF intensity envelope), intermediate- (650-850 cm^{-1}; MF intensity envelope) and high- (850-1250 cm^{-1}; HF intensity envelope) frequency ranges, respectively. In the raw spectra of water-poor HGG0 glasses, one narrow peak is observed at 490 ± 5 cm^{-1} (D1) superimposed on the major broad LF envelope (465 ± 5 cm^{-1}) and an additional shoulder, which peaks at 600 ± 5 cm^{-1} (D2), is observed on the high frequency part of the same envelope (Fig. 5a) (Pasquarello and Car, 1998; Ruiz et al., 2002, Thao To et al., 2008). The water region 3000-3700 cm^{-1} is characterized by a broad and asymmetric band in all HGG glasses that is attributed to the stretching of OH units with variable degrees of hydrogen bonding as will be discussed further (Behrens et al., 2006; Di Muro et al., 2006a) (Fig. 2).

Collected polarized spectra were used to guide the deconvolution of the HF envelope in unpolarized spectra, in order to describe the spectral evolution with pressure and water increase. Inspection of

shoulders occurring in both parallel (VV) and perpendicular (VH) polarized spectra constrains the adopted deconvolution strategy (Figs. 5, 6). Band positions, intensities and depolarization ratios were obtained as follows: The polarized MF and HF envelopes of water-poor and water-rich glasses quenched at low pressure were initially deconvoluted using 6 Gaussian bands, 5 bands corresponding to the HF envelope (as Seifert et al., 1982; Mysen and Frantz, 1994), in addition to a band at 800 cm^{-1} in the MF envelope taken as lower limit for the deconvolution. In a first step, all parameters were free and unconstrained in the fitting of the polarized spectra. We observe that the resulting frequencies of the deconvolution bands are very similar for water-poor and hydrous glasses. Therefore, the HF envelope of the unpolarized spectra was deconvoluted by maintaining deconvolution band position and width/intensity-ratio constant, only allowing for variation in the band relative intensity (Fig. 6). This strategy was chosen to minimize the error associated with deconvolution and to simplify comparison among spectra obtained at variable pressures and water contents (Fig. 6).

Deconvolution demonstrates that the main LF envelope and the D1 and D2 bands are highly polarized, whereas the band at 800 cm^{-1} in the MF spectral range is almost depolarized (ρ_{dr}= 0.30-0.18; Table 3). The HF intensity envelope has a variable degree of polarization that evolves with frequency and water content (Table 4). In the water-poor HGG0 glass, the high wavenumber region of the HF envelope (>1100 cm^{-1}) is highly polarized (ρ_{dr}=0.08; Table 4), whereas the low wavenumber region is only weakly polarized (ρ_{dr}=0.15-0.23) (Fig. 5a; Table 4). In the low wavenumber tail of the HF envelope, the slightly polarized deconvolution band centered at about 905 ± 10 cm^{-1} (ρ_{dr}=0.15; Table 4) is barely visible in the VV spectrum of water-poor glass but its intensity increases with water content (Fig. 5b). Depolarization ratios of deconvolution bands at 800 cm^{-1} and 905 cm^{-1} are similar in HGG0 and HGG3 glasses, but become 2-4 times higher for the other bands with increasing water contents. In HGG3, the high-wavenumber side becomes faintly polarized (ρ_{dr}= 0.20-0.17; Table 4), while the low-wavenumber side is depolarized (ρ_{dr}=0.55-0.20; Table 4). With increasing water contents, the peak position of the LF envelope shifts from 465 to 490 ± 5 cm^{-1} and merges with the D1 peak, while the D2 peak decreases in intensity (Fig. 5b). The observed evolution of the LF envelope could be produced by i) a decrease in D1 intensity and concomitant positive shift of the LF envelope or ii) a pronounced increase in D1 intensity with respect to the low frequency side of the main band. The LF envelope was not deconvoluted and only the evolution of the frequency, intensity and width of the experimental features will be described.

4.3.2. Raman band assignments

The structure of natural and synthetic aluminosilicate glasses can be schematically described as a statistical distribution of interconnected n-fold rings. For instance, the structures of remelted rhyolitic (Zotov et al. 1992) and alkali feldspar glasses (Taylor and Brown, 1979; Seifert et al., 1981, Seifert et al., 1982), whose composition is close to that of our glasses, is dominated by interconnected 6-membered rings. The sharp D1 and D2 defect bands observed in vitreous silica have been attributed to embedded populations of highly localized (*i.e.*, non-propagating) vibrational modes of regular rings with 3 and 4 members, respectively (Pasquarello and Car, 1998; Ruiz et al., 2002). Thao To et al. (2008) later attributed D1 to 3- and 4-membered rings and D2 to 3-membered rings.

In the Raman spectra of HGG glasses, the main and broad asymmetric LF envelope (150-650 cm^{-1}) is ascribed to delocalized vibrations of the aluminosilicate network that involve the displacement of bridging oxygen in intertetrahedral T-O-T linkages (McMillan et al., 1982). Specifically, the vibrations have been described either as symmetric oxygen stretching of the bent T-O-T linkages, with oxygen motion perpendicular to the T-T line, or as symmetric O-T-O angular deformation of the coupled TO_4 groups (Galeener and Geissberger, 1983; Sharma et al., 1984; McMillan and Hess, 1990; Ruiz et al., 2002). Spectral composition and width of the LF envelope are thus sensitive to both the average T-O-T intertetrahedral angle and the ring distribution statistics (Ruiz et al., 2002). A decrease in the average T-O-T bond angle and a change in ring statistics both concur in shifting to higher frequency and narrowing the LF envelope. Significant increase in the proportion of 4-membered rings at the expense of the largest ones is also a viable mechanism to produce the observed spectral evolution. With increasing depolymerization of the glass network, the observed LF envelope is expected to decrease in intensity relative to the HF envelope and to shift to higher frequency irrespective of the network modifying cations (Matson et al., 1983). In both synthetic and natural glasses, the LF/HF intensity ratio exponentially decreases with increasing glass depolymerization and increases with total dissolved water content (Mysen et al., 1980b; Di Muro et al., 2006b; 2009, Mercier et al., 2009).

The low intensity MF envelope (650-850 cm^{-1}) is attributed to the Si-O stretching mode (Kalampounias, et al., 2006) with a dominant Si motion (Matson et al., 1983), its intensity correlating with silica content (Seifert et al., 1982). The main feature of the envelope at 800 cm^{-1} contains two bands and was initially assigned to the TO-LO splitting, similarly to that observed in crystalline phases and glassy SiO_2 (Galeener, 1979), but later studies have challenged this interpretation (Galeener and Geissberger, 1983; McMillan et al. 1994). Kalampounias et al. (2006) described the network structure of potassium tetrasilicate glass/melt as a combination of tetrahedral units arranged in open (cristobalite-like at 790 cm^{-1}) and cluster (supertetrahedra at 830 cm^{-1}) substructures. As this feature appears insensitive to changes in pressure and water content (e.g., Fig.7), its behavior will not be discussed further and we will refer to it uniquely as a feature for the sake of clarity.

Conversely, the HF envelope provides information about the covalently bonded units, in Si-rich glasses, in terms of Q^n species, with *n* being the number of bridging oxygen: Q^4 at 1190 cm^{-1}, Q^3 at 1130 cm^{-1}, the band at 1045 cm^{-1} that may reflect the amount of Bridging Oxigens in the structure (BO; Mysen et al., 1980a), and Q^2 at 970 cm^{-1}. The assignment of the 900 cm^{-1} band is still debated (see discussion). In this frequency range, there are no Raman bands attributed to the vibration of network-modifying or charge-balancing cations in silica or alumino-silicate glasses. The specific effect of substituting Al for Si on the HF envelope is discussed in the section 5.1. The assignment of Raman bands proposed here is based on the close resemblance of HGG spectra (Figs. 1, 5, 6) with those of glasses and melts along the $(Na,K)AlO_2$-SiO_2 join, especially albitic glasses and the silica-rich glass AS50 (Seifert et al., 1982; Mysen et al., 1982; McMillan, 1984; Mysen, 1988; McMillan and Wolf, 1995; Poe et al., 2001; Shimoda et al., 2004).

The HGG0 glass was dehydrated and relaxed at 1 atm, but residual amounts of water are still observed in the high frequency domain of the Raman spectra. In this glass, a Raman band attributed to OH units peaks at 3506 ± 10 cm^{-1} and has an asymmetric negative skewed shape with a shoulder at 3740 ± 10 cm^{-1} (Fig. 7). Di Muro et al. (2006a) interpreted this polymodality as evidence of the presence of multiple OH sites with variable H-bonding. According to this interpretation the main shoulder is attributed to H-bonded OH units (Aines and Rossman, 1984; Mysen and Virgo, 1986), while the 3740 cm^{-1} shoulder can be ascribed to vibrations of "free" OH units (Di Muro et al., 2006a; Le Losq et al., 2013). or weakly H-bonded hydroxyl species, a feature that has been reported only in glasses with very low water contents (Di Muro et al., 2006a). In the hydrous glasses, an asymmetric high frequency envelope peaks at ca. 3575 cm^{-1} (Fig. 2). The shape and the spectral distribution of this broad envelope vary with the total dissolved water content and with the composition and structure of the glass (Mysen and Virgo, 1986; Di Muro et al., 2006a). The broad envelope does not allow a unique frequency identification for each species. Nevertheless, it is widely recognized that the lowest frequency features of the envelope (3300-3550 cm^{-1}) reflects the molecular water vibrations, whereas the higher frequency part (>3550 cm^{-1}) is related to the hydroxyl OH vibrations (Aines and Rossman, 1984; Mysen and Virgo, 1986). No tail is observed at the higher frequency side corresponding to the weakly free OH unit observed in natural glasses with less than 1 wt% dissolved water (Muro et al., 2006a).

4.4. Effect of pressure on water-poor glasses (HGG0)

The previous description of the spectral features of the water poor glass (HGG0) synthesized at 1 atm also applies to higher pressure syntheses (Fig. 7). The LF main envelope evolves with pressure, whereas changes in the MF and HF envelopes are less prominent. The LF intensity envelope

becomes progressively narrower and peaks at higher frequencies with increasing pressure (Fig. 7; Table 5). The FWHM* of the LF envelope was obtained as the width at half of the maximum height, without any specific deconvolution of the envelope (Fig. 8). The width of the LF envelope remains almost constant for the first pressure increment from 1 atm to 0.5 GPa but decreases by about 14% between 0.5 and 2.0 GPa, levelling off in the last pressure step to 2.5 GPa (Fig. 8). The experimental frequencies of the LF and HF envelopes (not deconvoluted) for all investigated compositions are reported as a function of pressure in Figure 9. The experimental frequency of the main envelope LF increases with pressure by 32 ± 5 cm^{-1} in our pressure range (1 atm to 2.5 GPa, Fig. 9a; Table 5). The D1 defect band becomes embedded in the LF envelope at pressures higher than 2.0 GPa and then cannot be unambiguously resolved from the main feature of the LF envelope (Fig. 7). In the pressure range lower than 2.0 GPa, the frequency of the D1 defect band remains constant (Fig. 9a). In all spectra, the D2 defect band remains visible as a shoulder whose intensity (normalized to that of the LF band) decreases slightly (ca. 10%) with pressure.

The experimental frequency of the main feature of the MF envelope remains almost constant at 800 ± 10 cm^{-1}. Its normalized intensity is constant up to 1.0 GPa but drops by 14% and then remains constant with further pressure increase (Fig. 7). Also the experimental frequency of the main feature of the HF envelope remains mostly constant at 1132 ± 3 cm^{-1} (Fig. 9d; Table 5). The only exception is for the glass synthesized at 0.5 GPa, in which the main feature of the HF envelope is located at slightly higher frequency (+1 %). The normalized intensity of this feature decreases linearly with pressure by about 15 % from 1 atm to 2.5 GPa (Fig. 9e). The spectral evolution of the HF envelope, deconvoluted as illustrated in Figure 6, shows that nearly anhydrous glasses have, within error, constant deconvoluted band areas up to 1.0 GPa (Fig. 10a). For the same composition, higher pressures decrease the deconvoluted area of the high frequency band at 1190 cm^{-1} but increase that of the 970 cm^{-1} band (Fig. 10a).

4.5. Effect of water at a constant pressure of 0.5 GPa

The spectra of HGG glasses with various water contents quenched at 0.5 GPa are compared in Fig. 11. This comparison is made initially for the low pressure range to discuss the effect of hydration separately from that of pressure. The effect of water depends on the frequency range considered. The main change in the spectra upon hydration is the appearance of a strong deconvolution band visible near 900 cm^{-1} (Fig. 6) that progressively increases in intensity with water content, although its experimental frequency remains constant within errors (Figs. 9c; 11). In addition, water dissolution results in a 6-12 % narrower (Fig. 8) and positively shifted (from 469 ± 5 to 485 ± 5 cm^{-1}) LF envelope compared to the HGG0 glass (Fig. 9a; Table 5) and in a decrease of the normalized

intensity of the HF envelope (Fig. 9e; Table 5) whereas the MF envelope remains unaffected. In all hydrous glasses, the position of the LF envelope is positively shifted by about 20 ± 4 cm^{-1} by the first water addition compared to HGG0, but then remains constant with further water addition (Fig. 9a; Table 5). The narrow defect band D1 cannot be resolved from the broad LF envelope of the water-rich glasses (Fig. 9a). The position of the HF envelope does not change significantly with increasing water content compared to the anhydrous samples (HGG0) while its normalized intensity decreases with initial addition of water, and remains almost constant at high water contents (Fig. 9e).

4.6. Combined effect of water and pressure

In comparison with HGG0 glasses, the spectra of hydrous glass sets (HGG3 - HGG5) display only minor changes with increasing pressure in the spectral features of the LF and MF envelopes but differences are more noticeable for the HF envelope (Fig. 12). In the HGG3 and HGG4 glass sets, increasing pressure narrows the LF envelope (see the evolution of FHMW in Fig. 8). In hydrous glasses, the weak D2 band decreases slightly (10% or less) in intensity, showing the most pronounced decrease with the first pressure increment from 0.5 to 1.0 GPa (Fig. 12). At 2.0 GPa, the frequency of the main feature of the LF envelope is similar in both water poor (HGG0) and water-rich glasses (Fig. 9a). The MF envelope remains at a constant position of 800 ± 10 cm^{-1} in the spectra of all hydrous glass (Figs. 7, 12).

In all series of hydrous glasses, the frequency of the peak observed in the HF envelope at ca. 1130 cm^{-1} displays a negative frequency shift with increasing pressure to 2.5 GPa (Fig. 12) that varies from 17 ± 10 cm^{-1} for the HGG3 series to 6 and 17 ± 10 $cm^{-1}$for the HGG4 and HGG5 glass sets, respectively (Figs. 9d, 12). In HGG3 glasses, the normalized intensity of the HF envelope decreases with increasing pressure from 1 atm to 1.5 GPa and from 2.0 to 2.5 GPa, displaying a similar behavior as the HGG0 set (Fig. 9e). Between 1.5 and 2.0 GPa an increase in the normalized intensities, which is directly related to the positive shift of the band, is observed. A continuous negative linear shift is observed only at P > 1.0 GPa in the HGG4 and HGG5 sets (Fig. 9e; Table 5).

Close inspection of the spectral evolution of the HF envelope prior to deconvolution reveals that the evolution of the spectra with pressure is not continuous and that distinct processes occur below and above 1.5 GPa, as already described for the water poor HGG0 set. The intensity of the slightly polarized deconvolution band near 900 cm^{-1} shows a positive correlation with total dissolved water content as reported by Sharma et al. (1997). In our HGG glasses the evolution of the 900 cm^{-1} band intensity with pressure changes at 1.5 GPa, in particular for the lower water content glasses (*i.e.*, HGG3, Fig. 9c). At P > 1.5 GPa, a decrease in intensity with pressure is observed in the HGG3 and HGG4 sets, while HGG5 intensities remain constant. Irrespective of the pressure dependence, the

900 cm^{-1} band is always most intense in the set with the highest water content. The spectral evolution of the HF envelope, indicated by the variation of the deconvolution band at 1045 cm^{-1} (Fig. 10b), shows small variations with pressure only above 1.0 GPa, suggesting that structural changes related to NBO-bonding only occur above this pressure threshold. Nearly anhydrous glasses display, within error, constant deconvoluted band areas to 1.0 GPa (Fig. 10a). Higher pressures decrease the area of the high frequency 1190 cm^{-1} deconvolution band but increase that of the 970 cm^{-1} deconvolution band (Fig. 10a). The HF envelope for the HGG3 glass displays a similar evolution with pressure, but variations are within experimental errors. The glasses with higher water contents (HGG4 and HGG5) show smaller variations with pressure that become apparent only above 1.5 GPa.

4.7. Effect of pressure on OH stretching bands

In the high-frequency range (3000-4000 cm^{-1}), HGG Raman spectra show a broad and asymmetric envelope. As in spectra of both natural and synthetic glasses and melts, the intensity (relative to the low-frequency envelopes) of this band envelope correlates positively with the total dissolved water content (Di Muro et al., 2006). The bands convoluted to form this intensity envelope are assigned to OH stretching vibrations in molecular water (H_2O_m) and hydroxyl groups (OH).

All investigated glass series display a shift of the envelope observed in the water stretching region towards lower frequencies with increasing pressure. This shift increases with the amount of dissolved water in the structure (Table 5, Fig. 7; 12). In the nearly anhydrous glasses, the envelope attributed to OH stretching exhibits two peaks, the most intense at 3506 cm^{-1} and a second one at 3740 cm^{-1}. The main shoulder shifts rapidly to 3447 ± 10 cm^{-1} as pressure increases from 1 atm to 0.5 GPa, then the shift rate with pressure decreases and at 2.5 GPa this band locates at 3424 ± 5 cm^{-1}. The less intense shoulder shifts to 3635 ± 10 cm^{-1} at 0.5 GPa and is not further affected by the additional pressure increase. We note that the shape of the water envelope is strongly modified by further dissolution of water into the structure. In our hydrous glasses (HGG3 – HGG 5), stretching vibrations of OH (hydroxyl) and H_2O_m (molecular water) are represented by a single and broad asymmetrical band at ca. 3570 cm^{-1}. In the HGG3 glass set (2.7 wt% H_2O), the frequency of the "total water" ($OH+H_2O_m$) Raman band is independent of pressure whereas in glasses with higher water contents, we observe a slightly negative shift of the band by about 10 cm^{-1} and 17 cm^{-1} for the HGG4 (3.63 wt% H_2O) and HGG5 (5.24 wt% H_2O) glass sets as pressure increases from 0.5 to 2.5 GPa (Table 5, Fig. 12). In the water-rich glasses HGG4 and HGG5, the rate of shift with pressures increases above 1.5 GPa.

5. DISCUSSION

5.1. Dry Haplogranite glass structure

Melts and glasses along the $(Na,K)AlO_2$-SiO_2 join consist of a three-dimensional array of interconnected silica and alumina tetrahedra where alkalis fully charge-balance the Al^{3+} cations substituting for Si^{4+} in 4-fold coordination (Mysen, 1988). Although the presence of non-bridging oxygens in our HGG compositions cannot be ruled out following previous studies on highly polymerized anhydrous alkali- and alkaline-earth aluminosilicate glasses and liquids (e.g., Toplis et al., 1997; Mysen and Toplis, 2007; Neuville et al., 2008), NMR studies performed on the HGG samples show that high coordinated Al remains below detection limit (1-2%), suggesting that NBOs are minor species on our samples (Malfait et al., 2012).

Two main groups of structural models have been proposed in the literature for $(Na,K)AlO_2$-SiO_2 glasses and are summarized here:

Type 1 models ("two-unit models"): the Raman spectrum of SiO_2 glass displays two depolarized bands at 1060 cm^{-1} (band A) and 1190 cm^{-1} (band B) that have been attributed to the stretch of Si-O° bonds in two units with different intertetrahedral angles in the three-dimensional network (Mysen et al., 1980a; Seifert et al., 1982). In this model, band *A* is associated with the small-angle unit and band *B* with the large-angle unit. Following Mysen et al. (1980a), the *A* and *B* depolarized bands are retained in the spectra of $(Na,K)AlO_2$-SiO_2 glasses and their position shifts toward lower frequencies with increasing temperature and Al/(Al+Si) ratio due to the elongation and weakening of T-O bonds upon substitution of Si by Al. The *A* and *B* bands correspond to vibrations of two distinct three-dimensional units with the *B* band being associated to the unit with higher Al/(Al+Si) ratio whose intensity is predicted to increase with pressure. Mysen et al. (1982) further extended this model by defining four deconvolution bands in the HF intensity envelope of glasses along the $NaAlO_2$-SiO_2, $CaAl_2O_4$-SiO_2, and $MgAl_2O_4$-SiO_2 joins. These four bands are centered at 1009 cm^{-1}, 1066 cm^{-1}, 1127 cm^{-1} and 1190 cm^{-1}, respectively, in the spectrum of AS50 glass (Mysen et al., 1982; Seifert et al., 1982) similar in composition to HGG0. In situ studies along the $NaAlSiO_2$-SiO_2 join (Neuville and Mysen, 1996) have shown that the *1190*/*1127* intensity ratio increases with temperature but decreases with pressure (Mysen et al., 1983). The 1190 cm^{-1} band should correspond to "expanded" Al-Si rings ("unit I") with large inter-tetrahedral angle, while the 1127 cm^{-1} band is interpreted as the vibration of "dense" Al-Si rings ("unit II") with small inter-tetrahedral angle.

Several observations indicate that this model cannot be fully applied to our haplogranite glasses: For instance, the 1190 and 1127 cm^{-1} bands are polarized in the almost dry HGG0 glasses but only moderately polarized in our hydrous glasses (Fig. 5; Tab. 4). The 1190 cm^{-1} band intensity decreases with pressure as predicted by the above model. Nevertheless, this decrease occurs only above a

threshold pressure of 0.5-1.0 GPa. Most important, a linear increase of the 1127 cm^{-1} band intensity with pressure is not observed for deconvoluted spectra, except perhaps in the HGG3 set (Fig. 10).

Type 2 models ("one-unit models"): In Al-bearing fully polymerized glasses, variably polarized deconvolution bands in the HF envelope are attributed to vibrations in rings (*i.e*. 6-membered rings in albite glass) whose frequency decrease with increasing Al/(Al+Si) ratio (McMillan et al., 1982; Sharma et al., 1997). In HGG, the polarization of the bands at 1190 cm^{-1} and 1140 cm^{-1} indicate that they correspond to symmetric stretching vibrations of Q^4(Si) and Q^4(1Al) units, respectively (Q^n: TO_4 units with T = Al, Si; *n*: number of bridging oxygens; the number in parenthesis indicates the number of oxygens Si tetrahedra share with Al tetrahedra). The depolarized nature of the bands at 1045 cm^{-1} and 970 cm^{-1} (Fig. 5; Table 4) indicates that they originate from anti-symmetric stretching vibrations of Q^4(2Al) and Q^4(0Al)=Q^4(Si) units, respectively (McMillan et al., 1992; Neuville and Mysen, 1996; Mysen, 1999). Furthermore, stretching vibrations of Q^n species result in strongly polarized bands at 950 (Q^2 units) and 1100 cm^{-1} (Q^3 units) (McMillan et al., 1992; Mysen and Frantz, 1993). The band at 1045 cm^{-1} has also been correlated with increasing amounts of NBO (McMillan and Wolf, 1995) and considered a doublet of Q^2 (Mysen, 1988; Malfait et al., 2008). These three highly polarized bands are not observed in the HGG glasses, suggesting that alkalis already fully balance the 4-fold coordinated Al and that increasing amounts of dissolved H do not create additional NBOs (Fig. 10). Hence, on the basis of the high frequency bands measured in HGG glasses, *model 2* is retained for the interpretation of the HGG glass structures presented below.

5.2. Evolution of haplogranite glass structure with pressure

On the basis of the above structural model, the spectroscopic observations and density data of the HGG glasses are interpreted in terms of 1) ring statistics (the relative proportions of inter-connected *n*-membered Al-Si rings) and average T-O-T intertetrahedral angle of each ring population, 2) Al/Si ratios in different units and 3) water speciation and hydrogen-bond strength.

5.2.1. Ring statistics and ring sizes

Upon compression, the T-O-T angle decreases and hence could lead to a modification of the ring statistics (Ruiz et al., 2002). Moreover, pressure can affect the intertetrahedral T-O-T angle by modifying the Al/Si ratio of a given ring population. These effects are not easily discriminated by

555 Raman spectroscopy. However, an evolution of ring statistics with increasing pressure and water
556 content is suggested by the topological evolution of the LF envelope, as detailed below.

557 In the water-poor HGG0 glasses, increasing pressure progressively decreases the intensity of the D2
558 shoulder. This spectral evolution likely reflects a relative decrease in abundance of the smallest (3-
559 membered) rings (Pasquarello and Car, 1998; Ruiz et al., 2002, Thao To et al., 2008). As previously
560 stated, the observed frequency increase in the peak of the LF envelope may result either from i) a
561 positive shift of its low frequency (465 cm^{-1}) side, associated or not with a decrease in D1 intensity,
562 or ii) from a decrease in intensity of the 450 cm^{-1} region and a significant and concomitant increase
563 in the intensity of the D1 band. The D1 feature correlates with the presence of both 3- and 4-
564 membered rings (Thao To et al., 2008). The decrease in the proportion of 3-membered rings, as
565 suggested by the evolution of the D2 band, should correlate with a decrease in D1 intensity, unless a
566 significant proportion of 4-membered rings is created at the expense of larger rings (n>4).
567 The Raman data do not allow clarifying whether the change in the proportion of small ring
568 populations is preceded by deformation of their internal angles. The almost constant frequencies of
569 both D1 and D2 bands observed in our water-poor glasses suggest an absence of deformation upon
570 pressurization to 2.5 GPa (Figs. 7, 9a). Average internal angles of ~136° and 128° for the small rings
571 were calculated from our data considering the position of the LF envelope following the model of
572 Ruiz et al. (2002). The negligible pressure-induced shift of the D1 (up to 2.0 GPa) and D2 bands (up
573 to 2.5 GPa) contrasts with the average shift of 5.2 cm^{-1}/GPa and 1.5 cm^{-1}/GPa reported for these
574 bands in the *in situ* high pressure Raman study of SiO_2 glasses by Champagnon et al. (2008).
575 Possibly, the progressive overlap of the D1 band and a positive shift of the 465 cm^{-1} band with
576 pressure masks the expected positive shift of the D1 band in our HGG spectra. This observation may
577 lend support to the hypothesis that the 465 cm^{-1} band moves to higher frequency with pressure.
578 Alternatively, the constant frequency may arise either from i) the very low compressibility of the
579 smaller rings, ii) from Al-Si substitution in 3- and 4-membered rings counterbalancing the net
580 pressure effect or iii) from a partial relaxation of the internal angle of small 3-4 membered rings upon
581 glass decompression during quench. Available data do not permit to discriminate between these
582 processes, even if we suspect that the poor compressibility of the small rings may play a dominant
583 role. A possible partial relaxation upon decompression should produce a broadening of the LF
584 envelope as significant changes in Al coordination with increasing pressure have been ruled out by
585 NMR analysis of the same samples (Malfait et al., 2012).
586 In the water-poor HGG0 glasses, the peak of the LF envelope shifts with pressure from 461 to 490
587 cm^{-1} (Figs. 7, 9a), i.e. 13 ± 3 cm^{-1}/GPa. This rate of shift is actually in good agreement with the 10.4
588 ± 0.8 cm^{-1}/GPa reported by Champagnon et al. (2008) for silica. We propose that this frequency
589 change records both the narrowing of the average T-O-T angle and a re-distribution of ring

populations, because of the decrease in relative proportion of the smallest rings (n=3). Both processes concur with the linear increase of density with pressure (Lipinska-Kalita et al., 2005).

In hydrous glasses, a slight negative shift of the LF envelope would be expected when the proportion of small-sized rings decreases with pressure (n = 3, 4). This shift cannot be resolved in our dataset. Alternatively, both the populations of very large rings (n > 6) and small rings (n= 3, 4) are affected resulting in the almost constant position of the peak of the LF envelope of the hydrous glasses. The latter would be supported by the shrinkage of the main LF envelope with pressure in all glass sets, suggesting that the width of the T-O-T angle distribution becomes narrower (Fig. 8). We propose that the disappearance of the large values in the angle distribution indicates a decrease in relative abundance of the largest rings (n>4) and is an important process of glass densification, independently of water content. In fact, the shrinkage of the LF envelope parallels the evolution of the bulk glass density with pressure. The specific evolution of 4-membered rings (increase at the expense of large rings or decrease, like the 3-membered rings) cannot be definitively resolved with the available data and requires further investigation.

5.2.2. Units with variable Al/Si ratio

In the water-poor HGG0 glasses, the HF envelope exhibits only minor changes with increasing pressure (Fig.7) while larger spectral changes and significant negative shifts occur in the hydrous glass sets (Figs.11, 12). These correspond to a relative decrease in intensity of the ~1190 cm^{-1} deconvolution band and a concomitant increase in the relative intensity of the 970 cm^{-1} deconvolution band for the intermediate water contents (e.g. HGG3, HGG4; Figs. 7, 10a, 13) at 0.5 GPa. As argued above, it can be excluded that these changes correspond to a decrease in the abundance of polymerized Q^4 units and a concomitant increase in depolymerized Q^2 units. Water addition may cause disorganization in the Si-Al rich domains without necessarily decreasing the degree of polymerization (Zotov et al., 1992). The variations observed in our hydrous glasses upon pressure increase could be interpreted as a reorganization or increase in order of the Si-Al domains in a given unit (Kohn et al., 1992). Accordingly, the observed small negative shift of the HF envelope (Fig. 9d) should mostly relate to an intensity decrease of its high frequency (1190 cm^{-1}) and an intensity increase of its low frequency component (970 cm^{-1}). The negative shift could also stem from a decrease of the average T-O-T angle and a consequent elongation and weakening of the T-O bonds (Lee et al., 2006) but none of this was observed in the LF envelope.

5.2.3. Water dissolution

Different mechanisms have been proposed for the incorporation of water in the silicate network. In depolymerized systems, water disrupts the T-O-T bonds and forms T-OH bonds (Xue and Kanzaki, 2008; Malfait et al. 2009). In polymerized systems, water dissolution mechanisms could occur *via* 1) rupture of the T-O-T bonds followed by the formation of Si-OH and minor Al-OH units, leading to a bulk network depolymerization (Xue and Kanzaki, 2008; Malfait et al. 2009); 2) bridging to alkalis and formation of M-OH bonding with M = Na, K, Ca or Mg (Kohn et al., 1989; 1992; Xue and Kanzaki, 2008); or 3) by formation of H_3O^+ that distorts the structure of the silicate (Sharma et al., 1996; 1997). In the water-rich HGG glasses, the D1 band cannot be resolved and the D2 band is much less intense with respect to the water-poor HGG0 glasses (Fig. 7). This observation may suggest that water dissolution destabilizes the small-sized rings (n=3). In all hydrous glasses, the LF feature envelope is located at higher but constant frequency (480 cm^{-1}, Fig.9a) with respect to the almost dry HGG0 glasses at 1 atm - 0.5 GPa (460-470 cm^{-1}). This suggests a smaller average T-O-T angle in hydrous glasses that correlates with the smaller $d\rho/dP$ at P > 1.5 GPa compared to their nearly anhydrous counterpart (Fig. 3a). Water dissolution clearly affects the distribution of T-O-T angles. We propose that both compression of internal angles and the modification of ring statistics concur in the frequency increase of the LF envelope. If our interpretation is correct, water dissolution has a similar role as pressure increase by favoring the decrease in the population of very large (higher than 6-membered) and very small (3-membered) ring types.

5.2.4 Hydrogen bonding strength

Spectroscopic data summarized above (*Type 2 model*) do not show conclusive evidence for an increase in the proportion of NBOs in highly polymerized systems such as HGG haplogranites upon water dissolution, as the addition of alkalis does (Kohn et al., 1989; Zotov et al., 1992). This interpretation is consistent with the absence of a positive shift of the LF envelope in our hydrous glasses (to be expected for the addition of alkalis as shown by Di Muro et al. (2006a)), and with the absence of an increase in the intensity of deconvolution bands that could be related to Q^3 units in the HF envelope with increasing water contents.

In our model proposed for the HGG glasses, water dissolves as i) molecular water, ii) alkali-OH complexes and iii) "bridging" OH groups, *i.e.*, protons attached to a bridging oxygen in T-O-T linkages. These observations do not rule out possible T-OH linkages as proposed by Malfait (2009). Moreover, it has been shown that water, as well as excess alkalis (Na_2O) lead to an increase in the Poisson's ratio of haplogranite glasses, hence suggesting a decrease in the degree of polymerization (Malfait and Sanchez-Valle, 2013). Further spectroscopic analyses are required to better understand

659 the mechanisms of water incorporation in haplogranite glasses. Kohn et al. (1992) suggest that the
660 non-linear dependence of viscosity on water content may be explained by assuming that bridging
661 hydroxyl groups have a larger effect on viscosity than molecular water. In Fig. 12, a decrease of the
662 asymmetry with water addition is observed at constant pressure. This reflects a possible decrease of
663 the OH/H_2O_m ratio with increasing total dissolved H_2O in agreement with previous studies (Dixon et
664 al., 1995; Zhang et al., 2003). Thus, the decrease in the OH/H_2O_m ratio with increasing bulk water
665 content (Stolper, 1982) is expected to reduce the effect of water on bulk viscosity. Our data suggest
666 that initial water dissolution operates on specific sites, and is efficient in decreasing the population of
667 both the very small and very large rings, probably due to the formation of water-rich domains as
668 reported by Zotov et al. (1992).
669 In the following discussion, we assume that even if the evolution of water speciation with pressure
670 may not be fully quenched, the main modifications on the network are still retained upon quench
671 (Table 4). The strength of the O-H linkage depends on the short-range environment around the OH^-
672 species and may evolve during melt/glass densification. This interpretation is based on the
673 observation of the parallel evolution of the intensity of the Raman envelopes at 900 cm^{-1} and 3600
674 cm^{-1} with pressure.
675 The structural origin of the 900 cm^{-1} Raman band in hydrous glasses is still debated. In alumino-
676 silicate glasses, a highly polarized band at this frequency has been attributed to vibration of $T\text{-}O^-$
677 bonds in Q^2 species (Mysen and Virgo, 1986). However, our depolarized Raman data exclude this
678 interpretation for the HGG glasses as its intensity decreases or is not affected with increasing
679 pressure (Fig. 9c). On the other hand, Sharma et al. (1996; 1997) ascribed this band to a vibration of
680 the silicate framework associated to an anti-symmetric mode of a T-O-T group. Recent NMR
681 investigations (Xue and Kanzaki, 2004, 2006, 2008; Xue, 2009) as well as Raman and IR studies
682 (McMillan et al., 1993; Malfait, 2009) on the SiO_2-$NaAlSiO_4$ and SiO_2-$NaAlSi_3O_8$ joins have
683 assigned this band to T-OH vibrations. Malfait (2009) observed a negative shift of both the 900 and
684 the 3600 cm^{-1} Raman bands accompanied by a negative shift with increasing pressure of the 4500
685 cm^{-1} band observed by FTIR. In HGG glasses, however, only the 3600 cm^{-1} band shifts whereas the
686 900 cm^{-1} band remains at a constant frequency.
687 The negative shift of the water combination band and the decrease in intensity of the 900 cm^{-1} band
688 may thus record a weakening of the O-H bond upon increasing pressure (Fig. 9c). The negative shift
689 of the water combination band occurs in both the nearly anhydrous HGG0 glass, in which only OH
690 units are expected, as well as in the hydrous HGG4 and HGG5 sets, where water is dissolved as
691 molecular and hydroxyl species (Stolper, 1982). The almost constant frequency of the 900 cm^{-1} band
692 could suggest that pressure does not induce significant changes on the possible Si-OH and/or Al-OH
693 linkages in the HGG glasses. According to this interpretation, the weakening of the O-H bond during

densification of the HGG haplogranite glasses would increase above a pressure threshold of ~ 1.5 GPa. We propose that the O-H weakening is related to increasing interaction of H with neighboring oxygen and to progressive partitioning of the H-bond on several anions (Sharma et al., 1996; 1997). If this interpretation is correct, our data suggest that the relaxation of the O-H bond is independent from and precedes the relaxation of the bulk glass structures. In other terms, relaxed O-H structures can coexist with quenched unrelaxed bulk silicate glass structures. The observation that the negative frequency shift of the O-H stretching envelope is quenched in most glasses suggests that the O-H bond weakens during compression, but that this process does not represent the elastic part of the densification process. Although Hui et al. (2009) proposed an increase of the OH/H_2O_m ratio with pressure, this is not consistent with the negative shift of the 3600 cm^{-1} band (Di Muro et al., 2006; Fig. 12) and with the small increase in V^*_{H2O} at the highest pressures of this study (Table 3).

5.3. Effect of structural changes on melt physical properties

The evolution with pressure of the density and viscosity of silicate melts relates to structural changes occurring upon densification of the silicate network (Kushiro, 1978). Allwardt et al. (2005, 2007) reported a nonlinear relationship of pressure and the increase in Al-coordination in depolymerized glasses and concluded that increasing Al-coordination is an important component for densification, especially at high densifications (>5%). However, an Al NMR study of our anhydrous and hydrous haplogranites do not show significant changes in Al-coordination with pressure to 3.5 GPa suggesting that changes in Al coordination do not play a major role in the densification of these glasses in this pressure range (Malfait et al., 2012). Hence, in our haplogranitic glasses the compaction of the structure upon pressure increase is achieved by topological arrangements. These include the reduction of the average inter-tetrahedral bond angle (Figs. 9a, 13) and possibly a redistribution of ring sizes (Figs. 8, 13), as identified in our study and by previous authors (Mysen et al., 1983; Poe et al., 2001; Seifert et al., 1982; Sharma et al., 1979). Water addition favors a reorganization of the ring sizes and average T-O-T angles at low pressure, these show small variations with pressure increase. Compaction is in this case accommodated by a small distortion of the rings and possible reorganization of the Al/Si rich domains.

The viscosity of melts displays a more complex relation with pressure at high temperature: the viscosity of more polymerized melts decreases with increasing pressure but increases with pressure for depolymerized compositions (e.g., Kushiro, 1976; 1978a; 1978b; Kushiro et al., 1976; Scarfe et al., 1979; McMillan and Wilding, 2009). The negative pressure dependence of viscosity has been explained by progressive increase of 5-fold coordinated Si and Al in densified melts (Kushiro, 1976, McMillan and Wilding, 2009). In high temperature anhydrous systems, Bottinga and Richet (1995)

observed a positive correlation of viscosity with both pressure and network modifier content. Ardia et al. (2008) have shown that the viscosity of dry rhyolite melts decreases linearly with pressure at high temperature (T>1000°C) whereas the viscosity of hydrous rhyolites decreases with pressure at high temperature but increases at low temperatures close to Tg (Ardia et al., 2008; Hui et al. 2009). Following Al NMR results on hydrous rhyolites that show a negligible increase in 5-fold coordinated Al up to 3.5 GPa (Malfait et al., 2012), we note that the anomalies in the pressure dependence of the viscosity of hydrous rhyolites cannot be fully explained by Al coordination changes. These anomalies could be interpreted as variations of the activation volume of viscosity (Va), representing the volume requirement for local motion and structural rearrangement (Ardia et al., 2008). In anhydrous glasses, the decrease in viscosity with pressure is larger in the low-pressure range with respect to higher pressures (i.e. $d\eta/dP$ decreases mostly at 1.0-1.5 GPa) (Ardia et al., 2008). In hydrous glasses, the viscosity increases with pressure and results in a positive $d\eta/dP$ (Hui et al., 2009). On the basis of our Raman results, we ascribe the changes of the pressure effect on viscosity to an evolution of the densification mechanisms operating at different pressures.

On the basis of our spectral data, we propose that in hydrous compositions increasing pressure triggers a reorganization of the Al- and Si-rich domains above 1.0-1.5 GPa. Malfait et al. (2012) only reported a slight increase in Al coordination in hydrous glasses above 1.5 GPa that would not be detectable in our Raman spectra. It is therefore plausible that this reorganization could result from an increase in Al coordination, which in turn affects the observed decrease in the densification rate with pressure. At higher pressures than explored here, possible modification of the network ring sizes and angles becomes less favorable in hydrous glasses, the increase in Al coordination being a more likely process for further compaction of the structure.

We have inferred that the compaction of the hydrous rhyolite network is mainly achieved by a redistribution and homogenization of ring sizes and a decrease of the average intertetrahedral angle at pressures below 1.5 GPa, whereas above this pressure, the dominant densification mechanism is the redistribution of Al/Si rich domains. The observed structural modifications are thus consistent with the increase of the activation energy of viscous flow for hydrous liquids with pressure through variation of the activation volume of viscosity.

6. CONCLUSION

The densification mechanisms of haplogranite glasses have been investigated as a function of water content and pressure using density measurements and Raman spectroscopy. The main conclusions are summarized in Fig. 13. Densities and derived molar volumes display a linear dependence on pressure for the nearly anhydrous glasses. The densities of hydrous glasses rapidly increase linearly

up to 1.5 GPa but the densification rate decreases above this pressure. Densification upon pressure increase is associated first with a slight decrease of the partial molar volume of water up to 1.0 GPa, followed by an increase above this pressure that correlates with the reported higher H_2O_m/OH^- ratio at high pressure. Almost anhydrous liquids accommodate the increase in compression by distortion of the silicate network, including namely changes in T-O-T angles and average ring sizes. Pressure increase leads to an increase of the ordering of the Si/Al domains in the network of the water-poor liquids. The effect of pressure on the viscosity of nearly anhydrous compositions is reduced at higher pressures by a reorganization of the network. Water dissolved into the glass structure reduces significantly the range of possible ring sizes. In the hydrous glasses, the increase in density is thus essentially accommodated by a reorganization of ring sizes to an average ring (i.e., 6-membered ring) without major variations on the average T-O-T angles.

Acknowledgements. This work was supported by grant TH-27/05-3 of ETH Zurich and by grant No. 2-77182.02 of the Swiss National Science Foundation. P. Ardia further thanks the "Doktorandenstipendium" of ETH Zurich for financial support. We also thank N. Métrich of the Pierre Süe laboratory (CEA, France) for substantial support and W.J. Malfait for discussion. The authors want to thank two anonymous reviewers and the AE Dr. Toplis for comments that helped to improve the manuscript.

References:

Acosta-Vigil, A., London, D., and Morgan VI, G. (2005) Contrasting interactions of sodium and potassium with H_2O in haplogranitic liquids and glasses at 200 MPa from hydration-diffusion experiments. *Contributions to Mineralogy and Petrology* **149**(3), 276–287.

Aines, R., and Rossman, G. (1984) Water in minerals? A peak in the infrared. *Journal of Geophysical Research* **89** 4059-4071.

Allwardt, J. R. and Poe, B. T. and Stebbins, J. F. (2005). The effect of fictive temperature on Al coordination in high-pressure (10 GPa) sodium aluminosilicate glasses. *American Mineralogist* **90** (8-9), 1453-1457.

Allwardt, J. R., Stebbins, J. F., Terasaki, H., Du, L. S., Frost, D. J., Withers, A. C., Hirschmann, M. M., Suzuki, A., and Ohtani, E. (2007). Effect of structural transitions on properties of high-pressure silicate melts: Al-27 NMR, glass densities, and melt viscosities. *American Mineralogist* **92**(7), 1093–1104.

Ardia, P., Giordano, D., and Schmidt, M.W. (2008). A model for the viscosity of rhyolite as a function of H_2O content and pressure: A calibration based on centrifuge piston cylinder experiments. *Geochimica et Cosmochimica Acta* **72** 6003–6023.

Behrens, H. and Schulze, F. (2003). Pressure dependence of melt viscosity in the system NaAlSi3O8-CaMgSi2O6. *American Mineralogist* **88** 1351–1363.

Behrens, H. and Stuke, A. (2003). Quantification of H2O contents in silicate glasses using IR spectroscopy - a calibration based on hydrous glasses analyzed by Karl-Fischer titration. *Glass Science and Technology* **76**(4) 176–189.

Behrens, H., Roux, J., Neuville, D., and Siemann, M. (2006). Quantification of dissolved H_2O in silicate glasses using confocal microRaman spectroscopy. *Chemical Geology* **229**(1-3) 96–

112.
Bottinga, Y. and Richet, P., (1995). Silicate melt structural relaxation: Rheology, kinetics, and Adam-Gibbs theory. *Geochimica et Cosmochimica Acta* **59** 2725-2731.
Brooker, M., Nielsen, O., Praestgaard E. (1988). Assessment of correction procedures for reduction of Raman spectra. *Journal of Raman spectroscopy* **19**(2) 71–78.
Champagnon, B., Panczer, G., Chemarin, C., and Humbert-Labeaumaz, B. (1996). Raman study of quartz amorphization by shock pressure. *Journal of non-crystalline solids* **196**(1-3) 221–226.
Champagnon, B., Martinet, C., Boudeulle, M., Vouagner, D., Coussa, C., Deschamps, T., and Grosvalet, L. (2008). High pressure elastic and plastic deformations of silica: In situ diamond anvil cell Raman experiments. *Journal of Non-Crystalline Solids* **354**(2-9) 569–573.
Del Gaudio, P. and Behrens, H. (2009). An experimental study on the pressure dependence of viscosity in silicate melts. *The Journal of Chemical Physics* **131** 1-14.
Di Muro, A., Villemant, B., Montagnac, G., Scaillet, B., and Reynard, B. (2006a). Quantification of water content and speciation in natural silicic glasses (phonolite, dacite, rhyolite) by confocal microRaman spectrometry. *Geochimica et Cosmochimica Acta* **70**(11) 2868–2884.
Di Muro, A., Giordano, D., Villemant, B., Montagnac, G., Scaillet, B., and Romano, C. (2006b). Influence of composition and thermal history of volcanic glasses on water content as determined by micro-Raman spectrometry. *Applied Geochemistry* **21**(5) 802–812.
Di Muro, A., Métrich, N., Mercier, M., Giordano, D., Massare, D., and Montagnac, G. (2009). Micro-Raman determination of iron redox state in dry natural glasses: Application to peralkaline rhyolites and basalts. *Chemical Geology* **259** 78-88.
Dingwell, D. B. and Webb, S. L. (1990). Relaxation in Silicate Melts. *European Journal of Mineralogy* **2**(4) 427–449.
Dingwell DB, Romano C, Hess KU (1996). The effect of water on the viscosity of a haplogranitic melt under P-T-X conditions relevant to silicic volcanism. *Contrib. Mineral. Petrol.* **124** 19-28.
Dixon, J.E., Stolper, E.M., Holloway, J.R (1995). An experimental study of water and carbon dioxide solubilities in mid ocean ridge basaltic liquids .1. Calibration and solubility models. *J. Petrol.*, **36**(6) 1607-1631.
Galeener, F. (1979). Band limits and the vibrational spectra of tetrahedral glasses. *Physical Review B*, **19**(8) 4292–4297.
Galeener, F. and Geissberger, A. (1983). Vibrational dynamics in ^{30}Si-substituted vitreous SiO_2 . *Physical Review B* **27**(10) 6199–6204.
Giordano, D and Nichols, ARL and Dingwell, DB (2005). Glass transition temperatures of natural hydrous melts: a relationship with shear viscosity and implications for the welding process. *Chemical Geology* **256**(3) 78-88 203-215. *J. Volcanol. Geotherm. Red.* **142**(1) 105-118.
Giordano, D., Russell, K., Dingwell, D.B. (2008a). Viscosity of magmatic liquids: a model. *Earth and Planetary Science Letters* **271** 123-134.
Giordano, D., Potuzak, M, Romano, C and Dingwell, DB and Nowak, M (2008b). Viscosity and glass transition temperature of hydrous melts in the system $CaAl_2Si_2O_8$-$CaMgSi_2O_6$. *Chemical Geology* **256**(3) 78-88 203-215.
Gottsmann, J., Giordano, D., and Dingwell, D. (2002). Predicting shear viscosity during volcanic processes at the glass transition: a calorimetric calibration. *Earth and Planetary Science Letters* **198**(3) 417–428.
Hess, K.-U. and Dingwell, D. (1996). Viscosities of hydrous leucogranitic melts: A non-Arrhenian model. *American Mineralogist* **81** 1297-1300.
Hochella, M. F. and Brown, G. E. (1985). The Structures of Albite and Jadeite Composition Glasses Quenched from High-Pressure. *Geochimica et Cosmochimica Acta* **49**(5) 1137–1142.
Holtz, F., Behrens, H., Dingwell, D., and Taylor, R. (1992). Water solubility in alumosilicate melts of haplogranite composition at 2 kbar *Chemical Geology* **96** 289–302.
Hui. H, Zhang Y., Behrens H. (2008). Pressure dependence of the speciation of dissolved water in rhyolitic melts. *Geochimica et Cosmochimica Acta* **72** 4756-4777.

Hui, H. and Zhang, Y. and Xu, Z. and Del Gaudio, P. and Behrens, H. (2009). Pressure dependence of viscosity of rhyolitic melts. *Geochimica et Cosmochimica Acta* **73** 3680-3693.

Kalampounias, A.G., Yannopoulos, S.N., and Papatheodorou, G.N. (2006) A high-temperature Raman spectroscopic investigation of the potassium tetrasilicate in glassy, supercooled, and liquid states: *The Journal of Chemical Physics*, 125 (16) 164502, doi: 10.1063/1.2360275.

Kohn, S. C., Dupree, R., and Smith, M. E. (1989). Proton environments and hydrogen-bonding in hydrous silicate-glasses from proton NMR. *Nature* **337** 539-541.

Kohn, S. C., Dupree, R., and Mortuza, M. (1992). The interaction between water and aluminosilicate magmas. *Chemical geology* **96**(3-4) 399–409.

Kushiro, I. (1976). Changes in Viscosity and Structure of Melt of $NaAlAi_2O_6$ Composition at high-pressures. *J. Geophys. Res.* **81** 6347–6350.

Kushiro, I. (1978). Viscosity and structural changes of Albite ($NaAlSi_3O_8$) melt at high pressures. *Earth and Planetary Science Letters* **41** 87-90.

Lange, R. A. and Carmichael, I. S. E. (1987). Densities of Na_2O-K_2O-CaO-MgO-FeO-Fe_2O_3-Al_2O_3-TiO_2-SiO_2 Liquids - New Measurements and Derived Partial Molar Properties. *Geochimica et Cosmochimica Acta* **51**(11) 2931–2946.

Lange, R. A. and Carmichael, I. S. E. (1989). Ferric-Ferrous Equilibria in Na_2O-FeO-Fe_2O_3-SiO_2 Melts- Effects of Analytical Techniques on Derived Partial Molar Volumes. *Geochimica et Cosmochimica Acta* **53**(9) 2195–2204.

Lee, S.K. , Cody, G.D., Fei, Y.W., Mysen, B.O. (2006). The effect of Na/Si on the structure of sodium silicate and aluminosilicate glasses quenched from melts at high pressure: A multi-nuclear (Al-27, Na-23, O-17) 1D and 2D solid-state NMR study. *Chem.Geol*. **229** (1-3) 162-172.

Le Losq, C., Moretti, R.; Neuville, D. R. (2013). Speciation and amphoteric behaviour of water in aluminosilicate melts and glasses: high-temperature Raman spectroscopy and reaction equilibria. Eur. J. Mineral. (25) 777–790.

Lipinska-Kalita, K.E., Gramsch, S.A., Kalita, P.E., and Hemley, R.J. (2005) In situ Raman scattering studies of high-pressure stability and transformations in the matrix of a nanostructured glass-ceramic composite. *Journal of Raman Spectroscopy* **36** 938–945.

Long, D.A. (1977). Raman spectroscopy. *McGraw-Hill New-York*, 204.

Long, D.A (2002). The Raman Effect: A Unified Treatment of the Theory of Raman Scattering by Molecules. Wiley.

Malfait W.J., Zakaznova-Herzog V.P., and Halter W.E. (2008) Quantitative Raman spectroscopy: speciation of sodium silicate glasses and melts. *American Mineralogist* **93** 1505-1518.

Malfait, W. (2009). The 4500 cm^{-1} infrared absorption band in hydrous aluminosilicate glasses is a combination band of the fundamental (Si,Al)-OH and O-H vibrations. *American Mineralogist* **94** 849–852.

Malfait, W.J., Sanchez-Valle C., Ardia P., Médard E., Lerch P. (2011) Compositionally dependent compressibility of dissolved water in silicate glasses. *American Mineralogist* **96** 1402-1409.

Malfait, W.J., Verel, R., Ardia, P, Sanchez-Valle, C. (2012) Aluminum coordination in rhyolite and andesite glasses and melts: effect of temperature, pressure, composition and water content. *Geochimica et Cosmochimica Acta* **77** 11-26, doi.org/10.1016/j.gca.2011.11.011.

Malfait, W.J. and Sanchez-Valle, C. (2013) Effect of water and network connectivity on glass elasticity and melt fragility, Chem.Geol. doi:10.1016/j.chemgeo.2012.04.034

Matson, D., Sharma, S., and Philpotts, J. (1983). The structure of high-silica alkali-silicate glasses. A Raman spectroscopic investigation. *Journal of non-crystalline solids* **58**(2-3) 323–352.

Matson, D., Sharma, S., Philpotts, J., (1986). Raman spectra of some tectosilicates and of glasses along the orthoclase-anorthite and nepheline-anorthite joins. *American Mineralogist* **71**, 694–704.

Maxwell, JC. (1867). On the dynamical theory of gases. Philosophical Transactions of the Royal Society of London, 157, 49-88.

McMillan, P. (1984). Structural studies of silicate glasses and melts; applications and limitations of

Raman spectroscopy? *American Mineralogist* **69**(7-8) 622–644.
McMillan, P. and Hess, A. (1990). Ab initio valence force field calculations for quartz. *Physics and Chemistry of Minerals* **17**(2) 97–107.
McMillan, P. and Wolf, G. (1995). Vibrational spectroscopy of silicate liquids. *Reviews in Mineralogy and Geochemistry* **32**(1), 247–315.
McMillan, P.F., Wilding, M.C. (2009). High pressure effects on liquid viscosity and glass transition behavior, polyamorphic phase transitions and structural properties of glasses and liquids. J. Non-Cryst. Sol. 355, 722-732.
McMillan, P., Piriou, B., and Navrotsky, A. (1982). A Raman spectroscopic study of glasses along the joins silica-calcium aluminate, silica-sodium aluminate, and silica-potassium aluminate. *Geochimica et Cosmochimica Acta* **46**(11) 2021–2037.
McMillan, P., Wolf, G., and Poe, B. (1992). Vibrational spectroscopy of silicate liquids and glasses. *Chemical Geology* **96**(3-4) 351–366.
McMillan, P., Poe, B., Stanton, T., and Remmele, R. (1993). A Raman spectroscopic study of H/D isotopically substituted hydrous aluminosilicate glasses. *Physics and Chemistry of Minerals* **19**(7) 454–459.
McMillan, P., Poe, B., Gillet, P., Reynard, B., (1994). A study of SiO2 glass and supercooled liquid to 1950 K via high-temperature Raman spectroscopy. *Geochimica et Cosmochimica* **58** 3653-3664.
McMillan, P. and Wilding, M.C. (2009) High pressure effects on liquid viscosity and glass transition behavior, polyamorphic phase transitions and structural properties of glasses and liquids. *J. of. Non-Crystalline Solids* **355**(10-12) 722-732.
Mercier, M., Muro, A. D., Giordano, D., Métrich, N., Lesne, P., Pichavant, M., Scaillet, B., Clocchiatti, R., and Montagnac, G. (2009). Influence of glass polymerisation and oxidation on micro-raman water analysis in alumino-silicate glasses. *Geochimica et Cosmochimica Acta* **73**(1) 197–217.
Morizet Y., Nichols A.R.L., Kohn C., Brooker RA., Dingwell, D.B. (2007). The influence of H_2O and CO_2 on the glass transition temperature: insights into the effects of volatiles on magma viscosity. *Eur. J. Mineral*. **19**(5) 657-669. DOI: 10.1127/0935-1221/2007/0019-1751
Moynihan C. T., Easteal A. J., Wilder J. and Tucker J. (1976) Dependence of the glass transition temperature on heating and cooling rate. J. Phys. Chem. 78, 2673–2677.
Moynihan, C.T. (1995). Structural relaxation and the glass transition. *Review in Mineralogy* **32** 1-19.
Mysen, B. O., Virgo, D., and Scarfe, C. M. (1980a). Relations between the Anionic Structure and Viscosity of Silicate Melts - a Raman-Spectroscopic Study. *American Mineralogist* **65**(7-8) 690-710.
Mysen, B. O., Virgo, D., Harrison, W. J., and Scarfe, C. M. (1980b). Solubility Mechanisms of H_2O in Silicate Melts at High-Pressures and Temperatures - a Raman-Spectroscopic Study. *American Mineralogist* **65**(9-10) 900–914.
Mysen, B.O., Finger, L.W., Virgo, D., and Seifert, F.A (1982) Curve-fitting of Raman spectra of silicate glasses. *American Mineralogist*. **67**. 686-695.
Mysen, B. O., Virgo, D., Danckwerth, P., Seifert, F. A., and Kushiro, I. (1983). Influence of Pressure on the Structure of Melts on the Joins NaAlO2-SiO2, CaAl2O4-SiO2, and MgAl2O4-SiO2. Neues Jahrbuch Fur Mineralogie-Abhandlungen, 147(3), 281–303.
Mysen, B. O. and Virgo, D. (1986). Volatiles in silicate melts at high pressure and temperature. II: Water in melts along the join NaAlO2 -SiO2 and a comparison of solubility mechanisms of water and fluorine. *Chemical Geology* **57**(3-4) 333–358.
Mysen, B. O. (1988). Structure and proprieties of Silicate Melts. Elsevier
Mysen, B.O. and Frantz, J. (1993). Structure and properties of alkali silicate melts at magmatic temperatures. *European Journal of Mineralogy* **5**(3) 393.
Mysen, B.O., and Frantz, J. (1994) Silicate melts at magmatic temperatures: in-situ structure determination to 1651° C and effect of temperature and bulk composition on the mixing behavior of structural units. *Contributions to Mineralogy and Petrology* **117** 1–14.

962 Mysen, B.O. (1999) Structure and properties of magmatic liquids: From haplobasalt to
963 haploandesite. *Geochimica et Cosmochimica Acta*, **63** 95–112.
964 Mysen, B.O., Toplis, M.J. (2007). Structural behavior of Al^{3+} in peralkaline, metaluminous, and
965 peraluminous silicate melts and glasses at ambient pressure. *American Mineralogist* **92** 933–
966 946.
967 Neuville, D. and Mysen, B. (1996). Role of aluminum in the silicate network: In situ, high-
968 temperature study of glasses and melts on the join SiO_2-$NaAlO_2$. *Geochimica et*
969 *Cosmochimica Acta* **60**(10) 1727-1737.
970 Neuville, D.R., Cormier, L., Montouillout, V., Florian, P., Millot, F., Rifflet, J.C., and Massiot, D.,
971 (2008) Amorphous materials: Properties, structure, and durability: Structure of Mg- and
972 Mg/Ca aluminosilicate glasses: 27Al NMR and Raman spectroscopy investigations.
973 *American Mineralogist* **93** 1721–1731.
974 Nielsen, O., Mortensen, A., Yarwood, J., and Shelley, V. (1996). Use of isotope effects in studies of
975 intermolecular interactions by Raman spectroscopy. *Journal of Molecular Structure* **378**(1)
976 1–9.
977 Ochs, F.A. III and Lange, R.A. (1999). The density of hydrous magmatic liquids. *Science* **283** 1314-
978 1317.
979 Okuno, M., Iwatsuki, H., and Matsumoto, T. (1996). Structural analysis of an obsidian by X-ray
980 diffraction method. *European Journal of Mineralogy* **8**(6) 1257–1264.
981 Okuno, M., Reynard, B., Shimada, Y., Syono, Y., and Willaime, C. (1999). A Raman spectroscopic
982 study of shock-wave densification of vitreous silica. *Physics and Chemistry of Minerals*
983 **26**(4), 304–311.
984 Pasquarello, A. and Car, R. (1998). Identification of Raman Defect Lines as Signatures of Ring
985 Structures in Vitreous Silica. *Physical Review Letters* **80**(23) 5145–5147.
986 Poe, B. T., Romano, C., Zotov, N., Cibin, G., and Marcelli, A. (2001). Compression mechanisms in
987 aluminosilicate melts: Raman and XANES spectroscopy of glasses quenched from pressures
988 up to 10 GPa. *Chemical Geology* **174**(1-3) 21–31.
989 Poe, B. T., Romano, C., Liebske, C., Rubie, D. C., Terasaki, H., Suzuki, A., and Funakoshi, K.
990 (2006). High-temperature viscosity measurements of hydrous albite liquid using in-situ
991 falling-sphere viscometry at 2.5 GPa. *Chemical Geology* **229**(1-3) 2–9.
992 Popel, P., Stankus, S., Mozgovoy, A., Khairulin, R., Pokrasin, M., Yagodin, D., Konstantinova, N.,
993 Borisenko, A., and Guzachev, M. (2011) Physical properties of heavy liquid-metal coolants
994 in a wide temperature range. *EPJ Web of Conferences* **15** 01014.
995 Reynard, B., Okuno, M., Shimada, Y., Syono, Y., and Willaime, C. (1999). A Raman spectroscopic
996 study of shock-wave densification of anorthite ($CaAl_2Si_2O_8$) glass. *Physics and Chemistry of*
997 *Minerals* **26**(6) 432–436.
998 Richet, P., Whittington, A., Holtz, F., Behrens, H., Ohlhorst, S., and Wilke, M. (2000). Water and the
999 density of silicate glasses. *Contributions to Mineralogy and Petrology* **138**(4) 337–347.
1000 Romano, C., Poe, B., Mincione, V., Hess, K., and Dingwell, D. (2001). The viscosities of dry and
1001 hydrous $XAlSi_3O_8$ (X= Li, Na, K, Ca 0.5, Mg 0.5) melts. *Chemical Geology* **174**(1-3), 115–
1002 132.
1003 Ruiz, F., Martìnez, J., and González-Hernández, J. (2002). A simple model to analyze vibrationally
1004 decoupled modes on SiO_2 glasses. *Journal of Molecular Structure* **641**(2-3) 243–250.
1005 Scherer, G. (1984). Use of the Adam-Gibbs equation in the analysis of structural relaxation. *Journal*
1006 *of the American Ceramic Society* **67**(7), 504–511.
1007 Schulze, F. and Behrens, H. and Holtz, F. and Roux, J. and Johannes, W. (1996). The influence of
1008 H_2O on the viscosity of haplogranitic melt. American *Mineralogist* **81** 1155-1165.
1009 Seifert, F., Mysen, B., Virgo, D., (1981). Structural Similarity of Glasses and Melts Relevant to
1010 Petrological Processes. *Geochimica et Cosmochimica Acta* **45** 1879-1884.
1011 Seifert, F., Mysen, B., and Virgo, D. (1982). Three-dimensional network structure of quenched melts
1012 (glass) in the systems SiO_2-$NaAlO_2$, SiO_2-$CaAl_2O_2$ and SiO_2-$MgAl_2O_4$. *American*
1013 *Mineralogist* **67**(7-8) 696–717.

Seifert, F. A., Mysen, B. O., and Virgo, D. (1983). Raman study of densified vitreous silica. *Physics and Chemistry of Glasses* **24** 141–145.
Sharma, S. K., Virgo, D., and Mysen, B. O. (1979). Raman Study of the Coordination of Aluminum in Jadeite Melts as a Function of Pressure. *American Mineralogist* **64**(7-8) 779–787.
Sharma, S., Matson, D., Philpotts, J., and Roush, T. (1984). Raman study of the structure of glasses along the join SiO_2-GeO_2. *J. Non-Cryst. Solids* **68**(1) 99–114.
Sharma, S., Wang, Z., and van der Laan, S. (1996). Raman Spectroscopy of Oxide Glasses at High Pressure and High Temperature. *J. Raman Spectrosc*., **27** 739–746.
Sharma, S., Cooney, T., and Wang, Z. (1997). Raman band assignments of silicate and germanate glasses using high-pressure and high-temperature spectral data. *J. Raman Spectrosc.* **28**(9) 697–709.
Shaw, H. (1963). Obsidian-H_2O Viscosities at 1000 and 2000 Bars in the temperature range 700 to 900°C. *Journal of Geophysical Research* **68** 6337–6343.
Shimoda, K., Okuno, M., Syono, Y., Kikuchi, M., Fukuoka, K., Koyano, M., and Katayama, S. (2004). Structural evolutions of an obsidian and its fused glass by shock-wave compression. *Physics and Chemistry of Minerals* **31**(8) 532–542.
Sipp, A. and Richet, P. (2002). Equivalence of volume, enthalpy and viscosity relaxation kinetics in glass-forming silicate liquids. *Journal of Non-Crystalline Solids* **298** 202-212.
Stevenson, R.J., Dingwell, D.B., Webb, S.L., Bagdassarov, N.S. (1995). The equivalence of enthalpy and shear stress relaxation in rhyolitic obsidian and quantification of the liquid–glass transition in volcanic processes. *J. Volcanol. Geotherm. Res.* **68**, 297– 306.
Stolper, E. (1982) The speciation of water in silicate melts. *Geochimica et Cosmochimica Acta* **46**(12) 2609–2620.
Suzuki, A., Ohtani, E., Funakoshi, K., Terasaki, H., and Kubo, T. (2002). Viscosity of albite melt at high pressure and high temperature. *Physics and Chemistry of Minerals* **29** 159–165.
Thao To, T., Bougeard, D , and Smirnov, KS. (2008) Molecular dynamics study of the vibrational pattern of ring structures in the Raman spectra of vitreous silica. *J. Raman Spectrosc*. 2008; **39** 1869–1877.
Taylor, M., Brown, G.E., Jr, (1979). Structure of mineral glasses-II. The SiO_2-$NaAlSiO_4$ join. *Geochimica et Cosmochimica Acta* **43** 1467–1473.
Tinker, D., Lesher, C., and Hutcheon, I. (2003), Self-diffusion of Si and O in diopside-anorthite melt at high pressures. *Geochimica et Cosmochimica Acta* **67** 133–142.
Toplis, M., Dingwell, D., Lenci, T. (1997). Peraluminous viscosity maxima in Na_2O-Al_2O_3-SiO_2 liquids: The role of triclusters in tectosilicate melts. *Geochimica et Cosmochimica Acta* **61** 2605–2612.
Toplis, M.J., Gottsmann, J., Knoche, R., Dingwell, D.B. (2001). Heat capacities of haplogranitic glasses and liquids. *Geochimica et Cosmochimica Acta* **65** 1985-2001.
Withers, A. and Behrens, H. (1999). Temperature-induced changes in the NIR spectra of hydrous albitic and rhyolitic glasses between 300 and 100 K. *Physics and Chemistry of Minerals* **27** 119–132.
Xue X. and KanzakiM. (2004) Dissolution mechanisms of water in depolymerized silicate melts: constraints from 1H and ^{29}Si NMR spectroscopy and ab initio calculations. *Geochimica et Cosmochimica Acta* **68** 5027–5057.
Xue X. and Kanzaki M. (2006) Depolymerization effect of water in aluminosilicate glasses: direct evidence from 1H–27Al heteronuclear correlation, NMR. *American Mineralogist* **91** 1922–1926.
Xue, X. and Kanzaki, (2008). M. Structure of hydrous aluminosilicate glasses along the diopside-anorthite join: A comprehensive one-and two-dimensional 1H and 27Al NMR study. *Geochimica et Cosmochimica Acta* **72** 2331-2348.
Xue, X. (2009) Water speciation in hydrous silicate and aluminosilicate glasses: Direct evidence from 29Si-1H and 27Al-1H double-resonance NMR. *American Mineralogist* **94** 395-398.
Zajacz, Z., Halter, W., Malfait, W., Bachmann, O., Bodnar, R., Hirschmann, M., Mandeville, C.,

Morizet, Y., Muentener, O., Ulmer, P., and Webster, J. (2005). A composition-independent quantitative determination of the water content in silicate glasses and silicate melt inclusions by confocal Raman spectroscopy. *Contribution to Mineral Petrology* **150**(6) 631–642.

Zhang, Y.X., Xu, Z.J., and Liu, Y. (2003). Viscosity of hydrous rhyolitic melts inferred from kinetic experiments, and a new viscosity model. *American Mineralogist* **88** 1741–1752.

Zotov, N., Yanev, Y., Epelbaum, M., and Konstantinov, L. (1992) Effect of Water on the Structure of Rhyolite Glasses - X-Ray-Diffraction and Raman-Spectroscopy Studies. *Journal of Non-Crystalline Solids* **142** 234–246.

Zotov N. and Keppler H. (1998) The influence of water on the structure of hydrous sodium tetrasilicate glasses. *American Mineralogist* **83** 823–834.

Zotov, N. (2003) Structure of natural volcanic glasses: diffraction versus spectroscopic perspective. *Journal of Non-Crystalline Solids* **323** 1–6.

Figure caption:

Fig. 1: Strategy for the treatment of Raman spectra in the spectral domain related to vibrations of the aluminosilicate framework: a) subtraction of the baseline (dotted) from the raw spectra; b) Long correction using Eq. 3, and c) normalization with respect to the highest peak of the LF envelope, smoothing of the data by using the Loess equation (3%) (line in c). See details in the text.

Fig. 2: Example of cubic baseline subtraction to the Raman spectral domain related to OH-stretching vibration (here the spectrum of the HGG5 glass at 0.5 GPa) and subsequent smoothing (grey line; Loess equation 3%).

Fig. 3: a) Measured densities vs. quench pressure for the synthesized HGG glasses and comparison with measured densities for dry albite glasses (Kushiro, 1976) and calculated densities for dry rhyolites quenched at 0.5 GPa using the pressure release technique (Withers and Behrens, 1999). Lines are guidelines and the arrow indicates the data point with the anomalously low density for HGG4 at 2.5 GPa discussed in the text. This glass is not considered for further discussion. b) Measured densities vs. water content for HGG and rhyolitic glasses at various pressures. The rhyolite glasses of Withers and Behrens (1999) were obtained by rapid quench (>100 °/s) with pressure release from 0.3 GPa (black stars) and by slow cooling (ca. 100-150 °/min) from 0.5 GPa (white stars). Errors of density measurement are smaller than symbol size.

Fig. 4: Molar volume of the haplogranitic matrix vs. total dissolved water in molar fraction (calculated as molecular water) at various pressures. Symbols are the calculated values for HGG at the corresponding pressure. Lines are fits at each pressure (0.5, 1.0, 1.5, and 2.5 GPa) assuming ideal mixing volumes. The fit lines yield the partial molar volume of the dry silicate (V_{sil}) and of water (V^*_{H2O}) as they intercept with the y-axis at 0 and 1, respectively (Table 3). Errors are calculated by propagating experimental errors in the density measurements.

Fig. 5: Unpolarized (black), parallel (VV, grey above), and perpendicular (VH, grey lower plot) polarized spectra of the nearly anhydrous composition at 1 atm (a), and (b) of the HGG3 glass with 2.7 wt% H_2O, synthesized at 0.5 GPa. Spectra are VV-polarized when the electric vectors of the incoming and scattered light are parallel and VH-polarized when they are perpendicular. Spectra were treated as illustrated in Fig. 1, without normalization and smoothing. Numbers in black indicate the frequency of the vibrational bands whereas the grey numbers in italic indicate experimental frequencies values of bands in the polarized spectra (Table 3). The difference in recorded intensity

between (a) and (b) is due to shorter acquisition time for the hydrous sample to avoid exsolution of H_2O.

Fig. 6: Deconvolution strategy for the HF envelope, normalized to the peak high of the LF envelope (Fig. 1), here applied to all the synthesized glasses at 0.5 GPa. Six deconvolution bands with fixed position and shape (width/intensity ratio, highlighted by the grey zones), imposed by the deconvolution of the polarized spectra (Fig. 5), are used to treat the HF envelope. The "PeakFit" software is used to optimize the r^2 value (min. 0.997) predefining the 6 deconvolution bands marked by the representative frequencies (see text). Generated line is created by the deconvolution strategy.

Fig. 7: Treated and smoothed spectra of the nearly anhydrous HGG0 glasses synthesized at different pressures. The dotted lines represent the frequencies of interest discussed in the text which values are given in italic. The most intense envelope (LF) shifts from 461 at room conditions (469 cm^{-1} at 0.5 GPa) to 493± 5 cm^{-1}, the HF envelope displays a slight negative shift from 1141 to 1133 cm^{-1} (± 10 cm^{-1}), and the main water band is negatively shifted from 3447 ± 10 cm^{-1} to 3424 ± 10 cm^{-1}. The four different spectral region discussed in the text are shown with different background colors.

Fig. 8: Full Width at Half Maximum (FWHM*) of the LF envelope (non smoothed) vs. pressure of glass synthesis. The width is measures at the half-height of the LF envelope, without any specific deconvolution of the envelope.

Fig. 9: Experimental frequencies and intensities of the normalized spectra (with Long correction, without smoothing) previous deconvolution vs. pressure. (a) position of the LF main envelope and of the D1 defect band only for HGG0 (crosses); (b) normalized intensity of the D2 band; (c) normalized intensity of the 900 cm^{-1} band for the hydrous glasses; (d) Frequency of the HF envelope; and (e) intensity of the HF envelope. Error on the frequency is ± 5 cm^{-1} for the LF spectral region and ± 10 cm^{-1} for HF region. The error for the intensities is calculated considering the variation of the intensities in the frequency errors.

Fig. 10: Spectral evolution of the HF envelope in terms of area variation of the deconvoluted bands (Fig. 6) vs. pressure in % deviation from the reference value of the glasses of the same composition synthesized at 0.5 GPa, here (a) for the nearly anhydrous glasses. (b) Deconvoluted band at 1045 cm^{-1}, NBO structure, for all the different glass compositions vs. pressure.

Fig. 11: Treated and smoothed spectra of all the investigated glasses synthesized at 0.5 GPa, with from the bottom to the top the increasing bulk water content. The vertical dotted lines represent the frequencies of interest discussed in the text, roman numbers in quotation marks depicting band labels, italic numbers accurate frequencies, both used in the text.

Fig. 12: Treated and smoothed spectra of the hydrous HGG glasses at different pressures. Vertical dotted lines identify the frequency values of the Raman bands of interest described in the text: LF main envelope (480 ± 5 cm^{-1}) and the shoulder formed by the D2 defect band (590 ± 5 cm^{-1}), the broad MF envelope at 800 cm^{-1}, the HF envelope with the band at 900 cm^{-1}, and the OH-stretching region at high frequencies. The numbers in italic are the effective experimental frequencies picked from the spectra (Table 5, error ± 5 for LF, ± 10 cm^{-1} for HF). Note the different x-axis scale of the low and high frequency sides.

Fig. 13: Schematic representation of the effect of pressure on the physical properties of water-poor (left) and water-rich (right) glasses. A) Viscosity η and T_g, B) density, C) evolution of the T-O-T mean angle, D) Al-coordination (Malfait et al., 2012); E) ring population. At the bottom (F), the pressure effect on the Raman water band, where the intensities of the water-poor Raman spectra (bottom left) were increased to highlight the band shifts. Viscosity is expressed as the value at T_{ae} close to the T_g.

Table 1

Table 1: Calculated quench temperature at viscosities of $10^{9.3}$ and 10^{12} Pa s.

		model:	Ardia et al., 2008	Hui et al., 2009	Ardia et al., 2008	Hui et al., 2009
sample	H_2O (wt%)	P (GPa)	T_{ae}(°C) h=$10^{9.3}$Pas		T_{ae}(°C)	h=10^{12} Pas
HGG0	0.15	1 atm	895	879	749	710
		0.5	873	874	731	714
		1.0	852	859	713	700
		1.5	830	838	695	675
		2.0	808	817	677	655
		2.5	786	798	659	640
HGG3	2.69	0.5	500	540	365	438
		1.0	478	545	347	444
		1.5	456	551	329	452
		2.0	435	560	311	463
		2.5	413	571	293	470
HGG4	3.63	0.5	440	502	309	405
		1.0	419	504	290	409
		1.5	397	509	272	416
		2.0	375	517	254	425
		2.5	353	526	236	436
HGG5	5.24	0.5	362	454	234	364
		1.0	340	453	216	365
		1.5	318	456	198	370
		2.0	297	462	180	377
		2.5	275	469	162	387

Table 2

Table 2: density and molar volume of HGG glasses at increasing water contents and quench pressures and calculated density at variou

		pyrex pycnometer - method 2						V[a] (cm^3/mol)		calculated		
	P (GPa)	#1	#2	#3	#4	average				WB 1999[b]	**T=25°C;P run[c]**	**T, P run[d]**
HGG0	0.0001	2.290	2.309	2.309	2.306	**2.305**	*9.0*	27.8	*2.3*		2.367	2.291
	0.5	2.340	2.338			**2.340**	*1.4*	27.4	*2.0*	2.387	2.457	2.376
	1.0	2.371	2.375			**2.374**	*2.8*	27.0	*2.1*		2.558	2.47
	1.5	2.409	2.411			**2.411**	*1.4*	26.6	*2.1*		2.668	2.572
	2.0	2.442	2.438	2.439		**2.441**	*2.1*	26.2	*2.1*		2.788	2.683
	2.5	2.491	2.479	2.488		**2.487**	*6.2*	25.7	*2.2*		2.919	2.804
HGG3	0.5	2.300	2.298	2.300	2.301	**2.301**	*1.3*	26.1	*2.0*	2.344	2.298	2.226
	1.0	2.346	2.347	2.347	2.346	**2.348**	*0.5*	25.6	*2.0*		2.382	2.305
	1.5	2.400	2.407	2.401	2.406	**2.405**	*3.5*	25.0	*2.1*		2.473	2.39
	2.0	n.a.									2.571	2.481
	2.5	2.434	2.435	2.436	2.435	**2.436**	*0.7*	24.7	*2.0*		2.677	2.58
HGG4	0.5	2.294	2.294	2.294	2.294	**2.295**	*0.3*	25.6	*2.0*	2.328	2.242	2.174
	1.0	2.336	2.339	2.336	2.338	**2.338**	*1.2*	25.1	*2.0*		2.321	2.248
	1.5	2.385	2.385	2.385	2.384	**2.386**	*0.5*	24.6	*2.0*		2.405	2.327
	2.0	n.a.									2.496	2.412
	2.5	2.366	2.369	2.366	2.368	**2.368**	*1.5*	24.8	*2.0*		2.594	2.503
HGG5	0.5	2.261	2.258	2.260	2.258	**2.260**	*1.5*	25.1	*2.0*	2.301	2.154	2.091
	1.0	2.317	2.314	2.316	2.314	**2.316**	*1.5*	24.5	*2.0*		2.224	2.157
	1.5	2.325	2.327	2.324	2.327	**2.327**	*1.5*	24.3	*2.0*		2.299	2.227
	2.0	n.a.									2.379	2.303
	2.5	2.376	2.377	2.375	2.379	**2.378**	*1.8*	23.8	*2.0*		2.466	2.383

errors are given in italic on the last digit number.

a) molar volume calculated as described by Richet et al. (2000) (assuming water as H_2O).

b) calculated as indicated by Withers and Behrens (1999) for rhyolitic glasses quenched at 0.5 GPa with a T ramp of 200°/min.

c, and d) calculated following Lange and coworkers (Lange and Carmichael, 1987; Lange, 1996; 1997; Ochs and Lange, 1999).

Table 4

Table 4: Deconvolution and depolarization ratios of HF bands.

	HGG0; 0.15 wt% H_2O					HGG3; 2.69 wt% H_2O				
	VV					**VV**				
Peak	Center[a]	FWHM	% Area	dep ratio		Center[a]	FWHM	% Area	dep ratio	
1	801	94	24.4	0.179	faint pol.	799	94	23.9	0.296	dep.
2	904	61	4.8	0.151	faint pol.	907	87	18	0.19	faint pol.
3	980	95	10.2	0.147	faint pol.	982	92	10.6	0.552	dep.
4	1059	97	21.5	0.227	faint pol.	1044	90	12.4	0.476	dep.
5	1133	82	24.5	0.082	pol.	1126	106	25	0.204	faint pol.
6	1191	77	14.6	0.082	pol.	1187	98	10.1	0.174	faint pol.
	VH					**VH**				
1	796	84	24.8			794	84	19.9		
2	917	97	7.3			902	83	10.3		
3	977	85	8.5			977	92	18.5		
4	1040	101	32.3			1047	80	16.6		
5	1140	113	17.7			1140	126	19.2		
6	1186	95	9.4			1197	274	15.5		

a) position of the band in cm^{-1} (+/- 10 cm^{-1}).

Table 5

Table 5: Raman band position of the HGG glasses at increasing water contents and quench pressures.

		LF region (± 5 cm^{-1})			HF region (± 10 cm^{-1})		water band (± 10 cm^{-1})	
	P (GPa)	LF band	D2	D2 - smooth[b]	1050 shoulder	HF band	peak pos.	H_2O tot[a]
HGG0	0.0001	461	595	591	1052	1130	3506[c]	0.15
	0.5	469	596	590	1049	1141	3447[c]	0.15
	1.0	468	594	590	1055	1132	3459[c]	0.13
	1.5	474	596	590	1047	1129	3434[c]	
	2.0	482	596	590	1051	1135	3421[c]	
	2.5	493	594	590	1053	1133	3424[c]	
HGG3	0.5	485	583	590	1056	1138	3577	
	1.0	483	581	590	1047	1143	3581	
	1.5	486	578	590	1044	1133	3568	
	2.0	482	581	590	1038	1126	3573	
	2.5	482	581	590	1053	1134	3575	
HGG4	0.5	488	574	590	1053	1138	3580	
	1.0	483	576	593	1049	1134	3578	
	1.5	488		590	1048	1133	3577	
	2.0	486		590	1053	1132	3570	
	2.5[d]	486		590	1048	1124	3563	
HGG5	0.5	483		584	1057	1138	3574	
	1.0	485		587	1057	1130	3570	
	1.5	483		590	1053	1132	3567	
	2.0	488		590	1049	1129	3564	
	2.5	486		590	1036	1121	3557	

a) water content calculated by internal calibration, see di Muro et al. (2006a)
b) D2 frequency after smoothing
c) highest peak after smoothing, related error is ± 8 cm^{-1}.
d) not considered for the discussion.

Table 3

Table 3: Molar volume of dry silicate and partial molar volume of molecular water

	P (GPa)	V_{sil}		V^*_{H2O}	
HGG at P:					
	0.50	27.42	*22*	12.82	*100*
	1.00	27.04	*20*	11.23	*100*
	1.50	26.49	*33*	12.17	*100*
	2.50	25.79	*30*	13.74	*100*
literature data:					
Ab/O	0.01-0.4	27.49	*1*	11.22	*28*
Ab/S-BP	0.1-0.7	26.29	*10*	14.54	*36*
Or	2	27.95	*14*	15.15	*90*
Hapl/D	0.04-0.33	26.71	*9*	13.33	*58*
RhyoK/S	0.11-0.45	27.55	*10*	11.37	*109*
RhyoP/S	0.07-0.51	27.55	*4*	11.24	*37*
Rhyo/Oc	0.02-0.59	26.28	*15*	12.55	*137*

error in italic is based on the last digit.
literature data are summerized by Richet et al. (2000). In detail: Ab/O: Orlova (1963), Ab/S-BP: Silver and Stolper (1989), Or, RhyoK/S, Rhyo/P/S: Silver et al. (1990), Hapl/D: Dingwell et al. (1996), and Rhyo/Oc: Ochs and Lange (1999).

Figure 1 Fig. 1

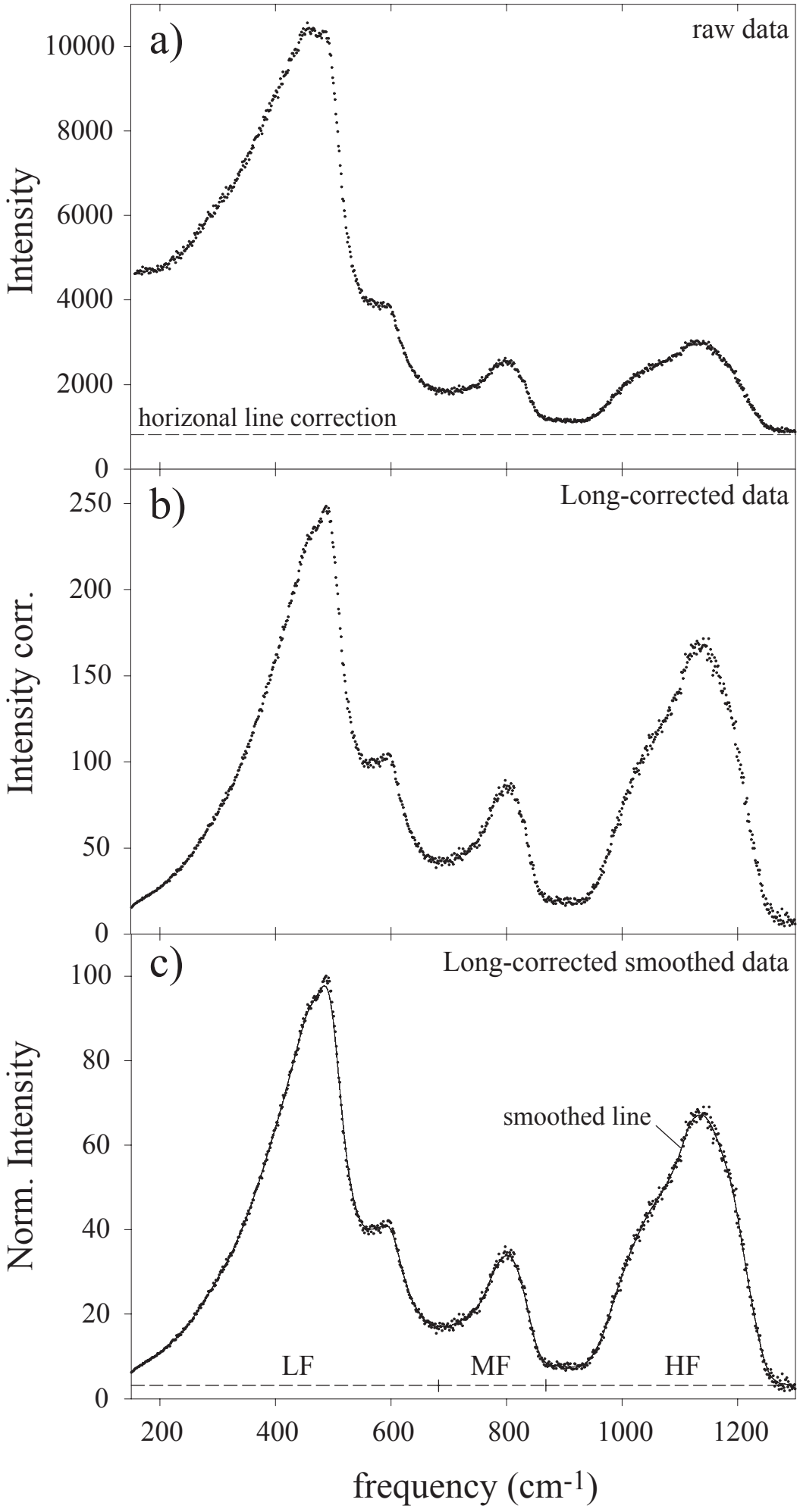

Figure 2 Fig. 2

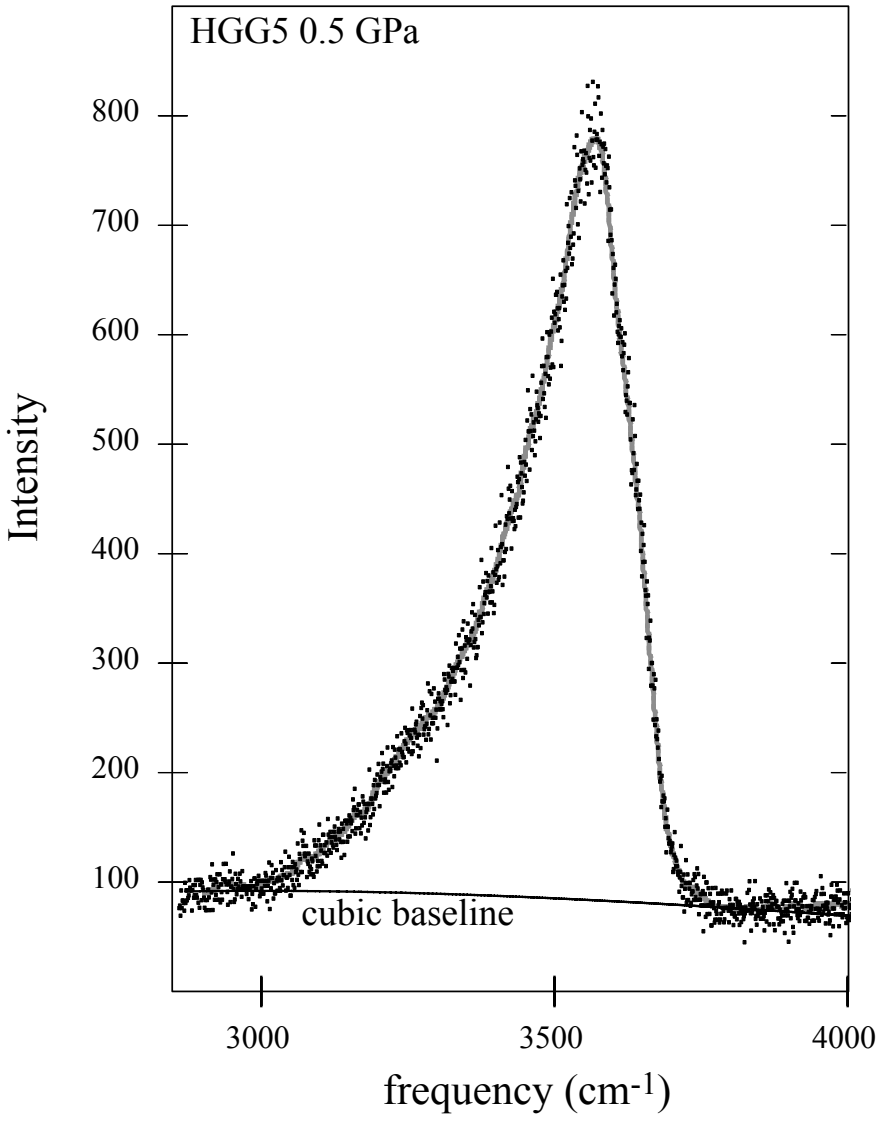

Figure 3
Click here to download high resolution image

Fig. 3

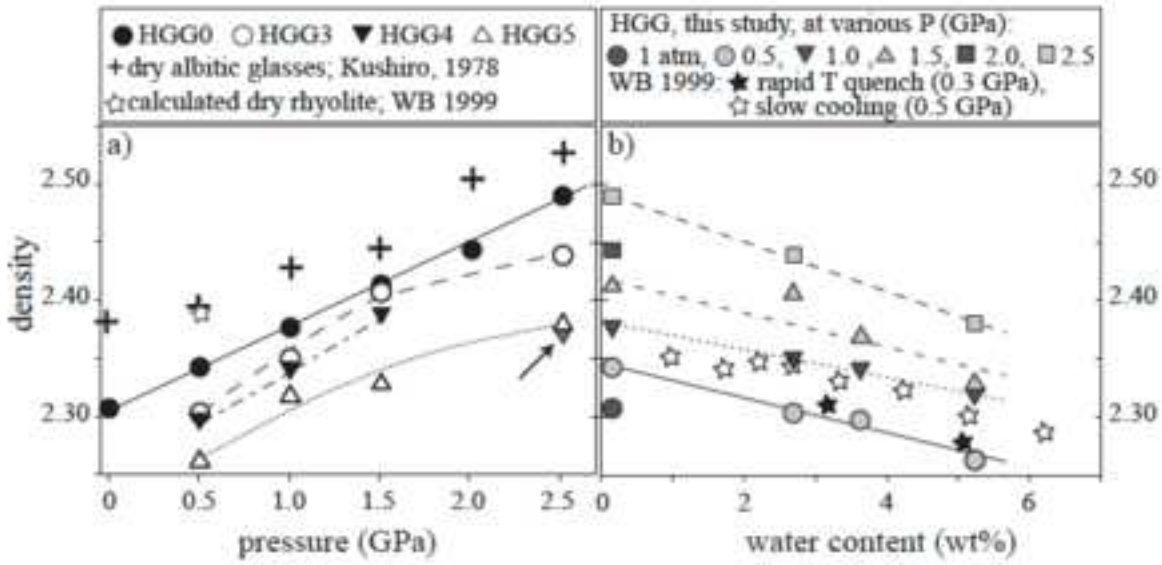

Figure 4 Fig. 4

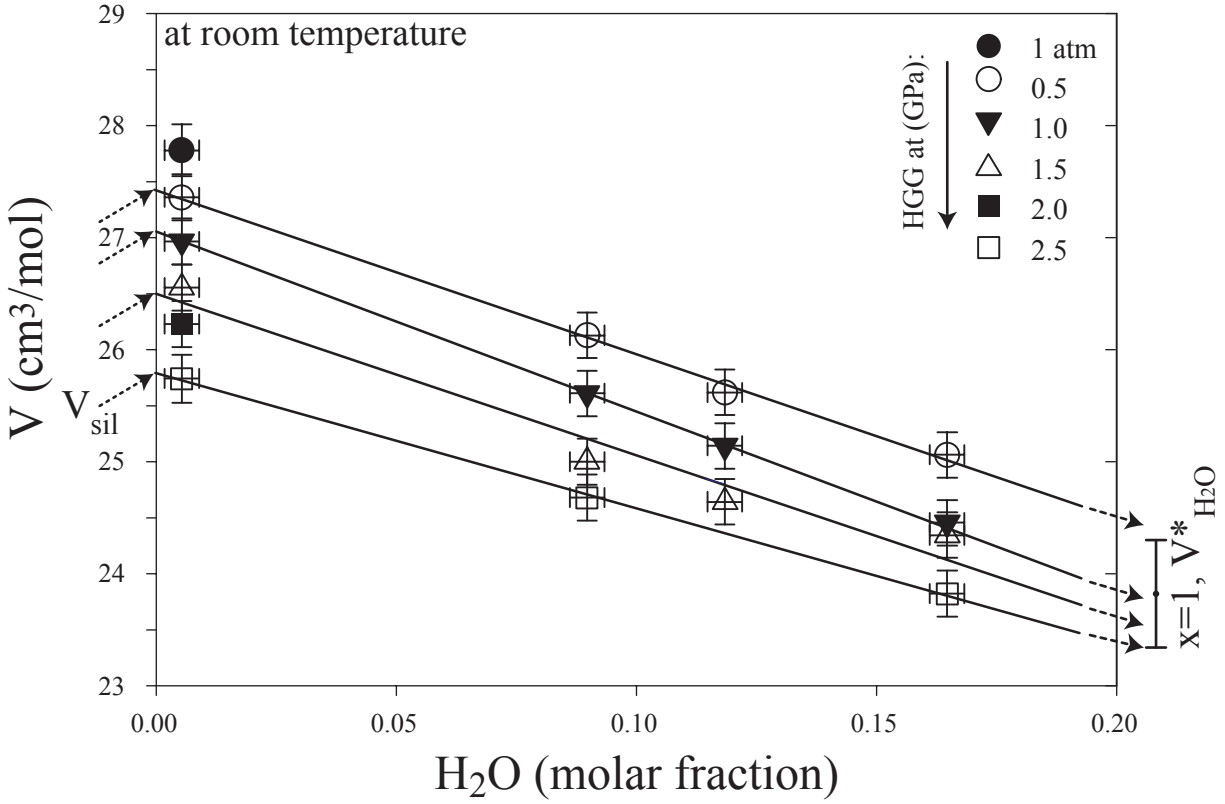

Figure 5 Fig. 5

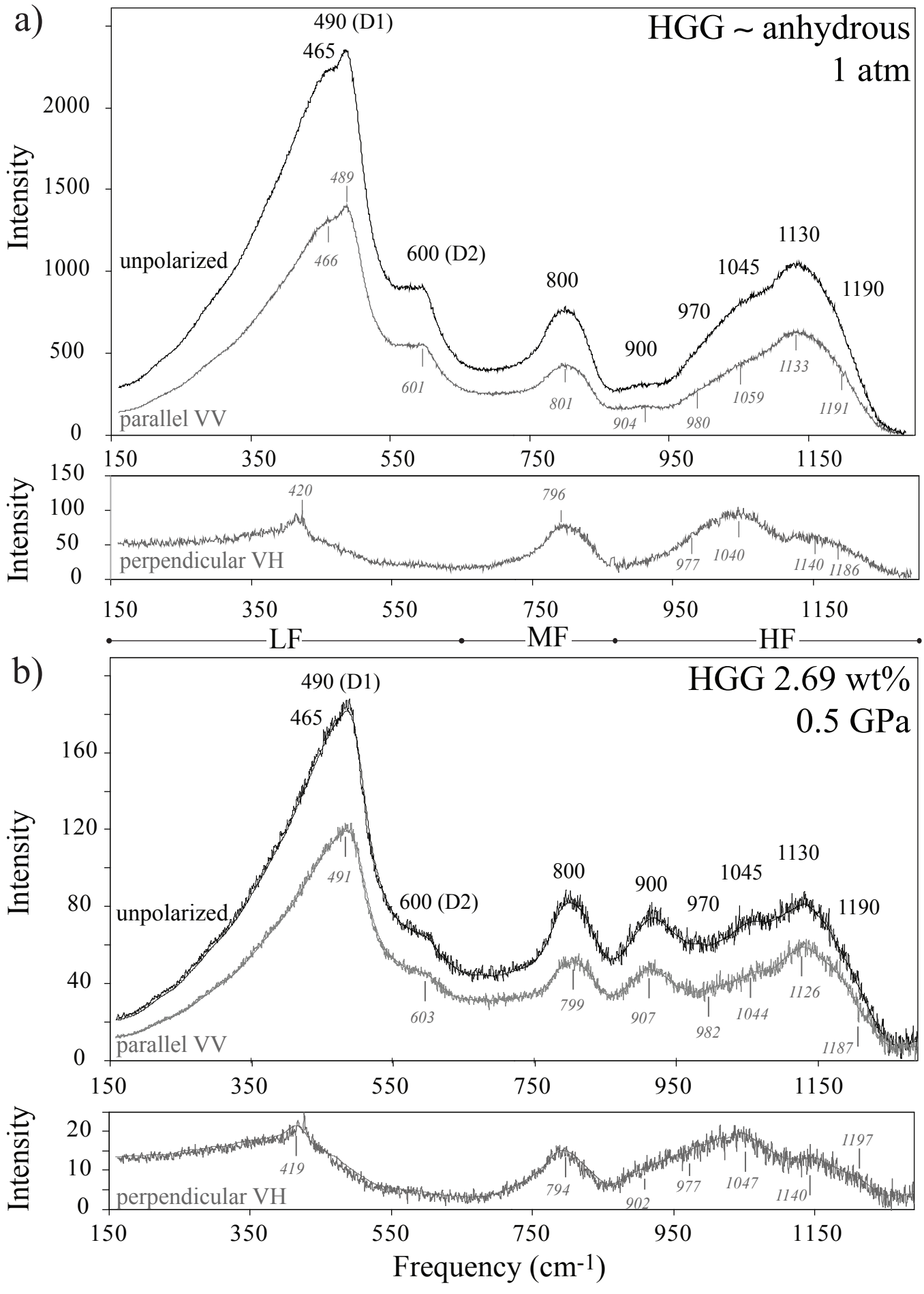

Figure 6 Fig. 6

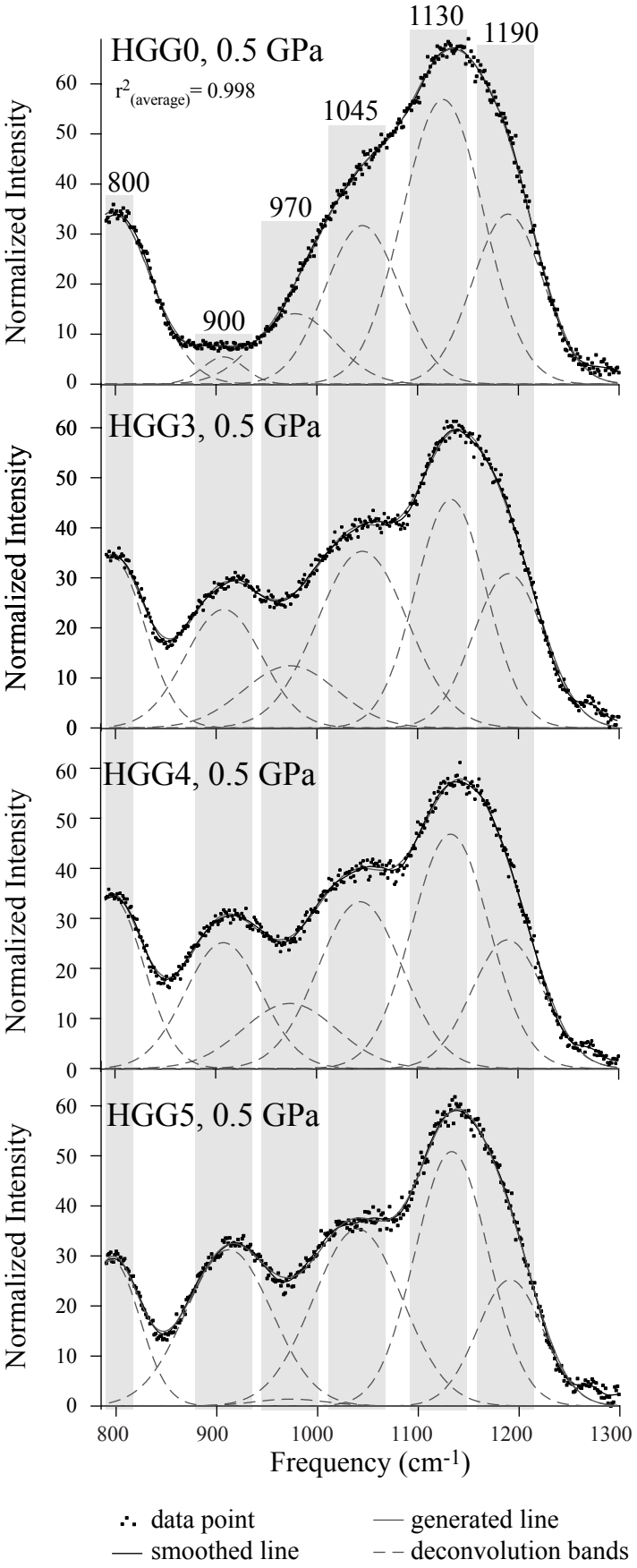

Figure Fig. 7

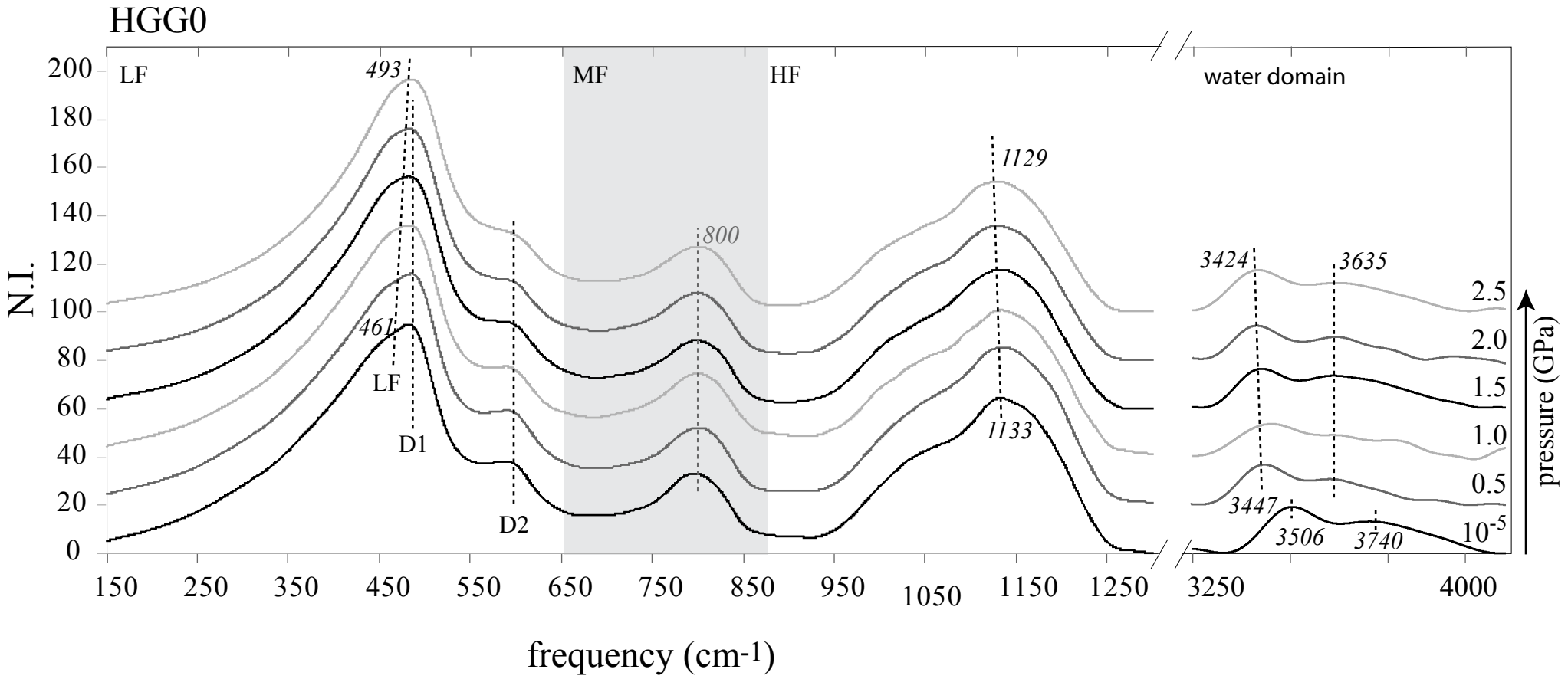
HGG0
LF
MF
HF
water domain
493
800
1129
461
LF
D1
D2
1133
3424
3635
3447
3506
3740
2.5
2.0
1.5
1.0
0.5
10-5
pressure (GPa)
N.I.
frequency (cm-1)

Figure 8 Fig. 8

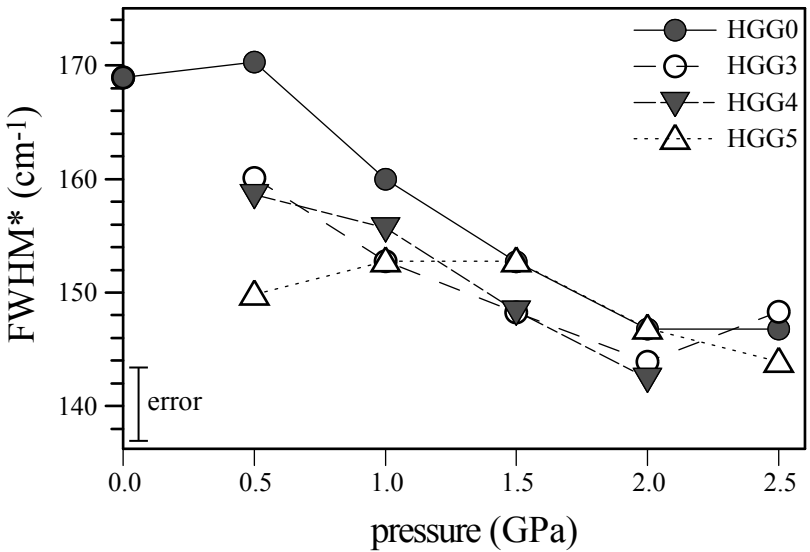

Figure 9 Fig. 9

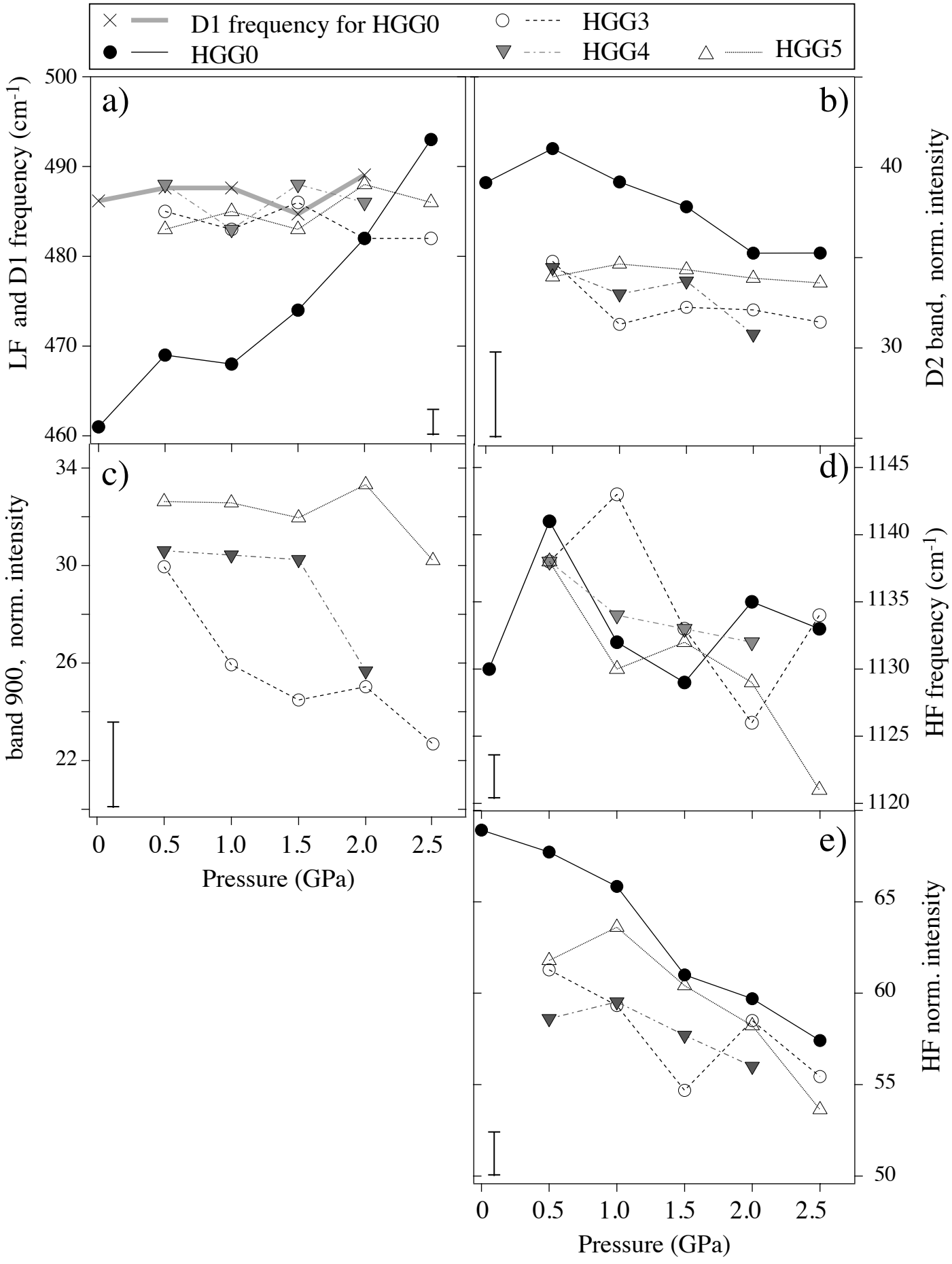

Figure 10
Click here to download high resolution image

Fig. 10

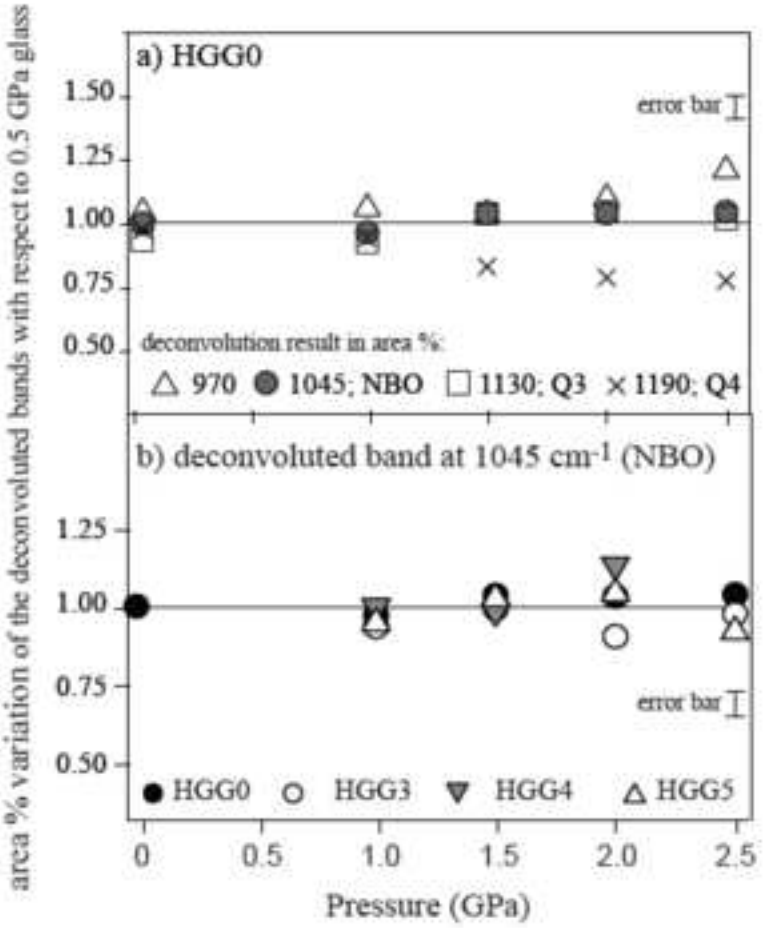

Figure 11

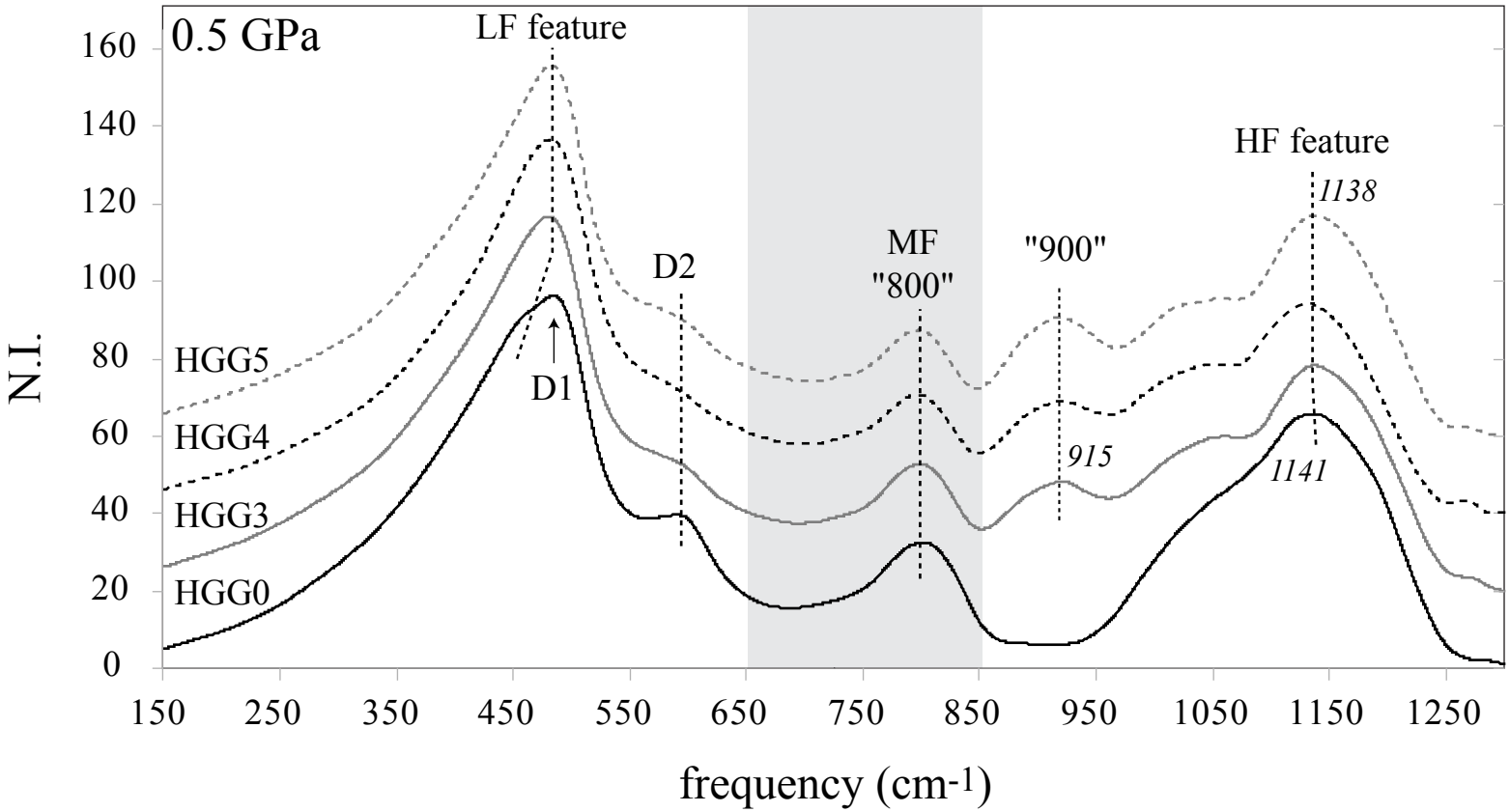
0.5 GPa
LF feature
HF feature
1138
MF
"800"
"900"
D2
D1
915
1141
HGG5
HGG4
HGG3
HGG0
N.I.
160
140
120
100
80
60
40
20
0
150
250
350
450
550
650
750
850
950
1050
1150
1250
frequency (cm-1)

Figure 12

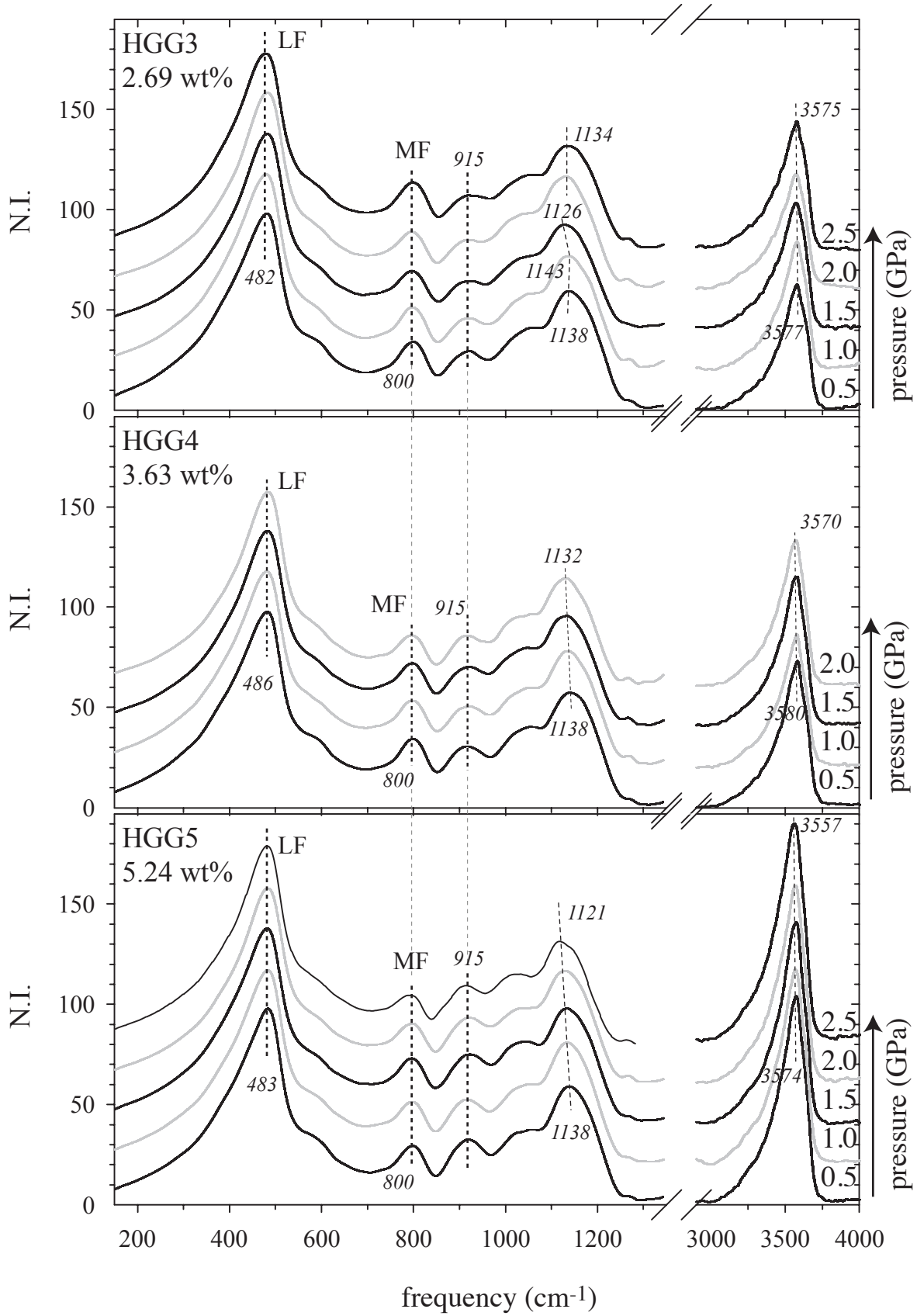
HGG3
2.69 wt%
LF
MF
915
1134
1126
1143
1138
482
800
3575
3577
HGG4
3.63 wt%
LF
MF
915
1132
1138
486
800
3570
3580
HGG5
5.24 wt%
LF
MF
915
1121
1138
483
800
3557
3574
N.I.
pressure (GPa)
0.5
1.0
1.5
2.0
2.5
0
50
100
150
200
400
600
800
1000
1200
3000
3500
4000
frequency (cm-1)

Figure 13. Fig. 13